Spark ignition engine performance, standard emissions and particulates using GDI, PFI-CNG and DI-CNG systems

Fuel 293 (2021) 120454

Contents lists available at ScienceDirect

Fuel

journal homepage: www.elsevier.com/locate/fuel

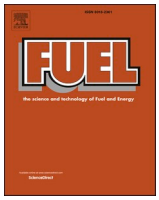

Full Length Article

Spark ignition engine performance, standard emissions and particulates using GDI, PFI-CNG and DI-CNG systems

Mindaugas Melaika [a,*], Gilles Herbillon [b,*], Petter Dahlander [a,*]

[a] Chalmers University of Technology, Hörsalsvägen 7A, 412 96 Gothenburg, Sweden
[b] GDTech, Avenue de l'Expansion 7, 4432 Alleur, Belgium

ARTICLE INFO

Keywords:
Spark ignition engine
Natural gas
Biogas
Direct injection
Port fuel injection
Standard emissions and particulates

ABSTRACT

Gaseous fuels, e.g., natural gas, biogas, have several advantages over liquid fuels owing to their favorable physical and chemical properties, e.g., lower carbon numbers in the fuel composition and no issues regarding fuel evaporation. The present study investigated compressed natural gas (CNG) port fuel injection (PFI) and direct injection (DI) systems compared to gasoline direct injection (GDI) cases in a spark ignition (SI) naturally aspirated single cylinder engine at stoichiometric conditions. The tests included usual engine working points – from 4.5 bar IMEP to 9 bar IMEP engine load at different engine speeds – from 1500 rpm to 2500 rpm. The main aim was to investigate how gaseous fuels can improve the SI engine efficiency, reduce standard emissions and particulates, and explain the benefits of a natural gas DI system versus standard gas PFI and GDI systems. Analysis of the results showed that the rate of heat release of natural gas was lower than that of gasoline fuel. However, the stable combustion process of DI-CNG gave additional benefits, e.g., increased turbulence in the cylinder, which increased the combustion rate and affected the exhaust gas formation. The highest engine efficiency was achieved with the same natural gas DI system. The highest iSHC, iSCO, $iSCO_2$ and $iSNO_x$ emissions reduction achieved at low and part load conditions with DI-CNG compared to GDI combustion. Particulates formation was lower with the gaseous fuel compared to gasoline. Additional benefits of lower particulate numbers among three injection systems were observed with DI-CNG combustion.

1. Introduction

Over the last few decades, many different alternative and renewable fuel types in the liquid (ethanol, RME, HVO, etc.) or gaseous (LPG, CNG, LNG, biogas/biomethane, etc.) phase have been investigated as alternatives in internal combustion engines (ICEs) to replace standard fossil fuels, i.e., gasoline and diesel. The search for alternatives was prompted by the need for reductions in CO_2 and other harmful exhaust gas emissions, e.g., hydrocarbons, carbon monoxide (CO), nitrous oxide (NO_x) and particulate matter (PM). Euro standards for exhaust gas emissions started to appear in the early 1990. Nowadays, emission standards are applied across the World with different limitation levels depending on the region or country. Recent exhaust gas emission standards in the European Union (EU) for light duty (LD) vehicles specify that CO_2 emissions should be reduced below 95 g/km by 2021, corresponding to 4.1 L/100 km for gasoline and 3.6 L/100 km for diesel fueled vehicles [1]. A further EU policy notes that CO_2 emissions must be reduced to below 81 g CO_2/km by 2025 and 59 g CO_2/km by 2030 based on the Worldwide harmonized Light Vehicles Test Procedure (WLTP) driving cycle [2]. The United States has set similar limitations for CO_2 emissions of 98 g/km after 2020 and 89 g/km of CO_2 after 2025 [3]. Other standard emissions in the EU are also strictly limited. The recent Euro 6 standard specifies limitations for passenger cars of up to 1 g/km for CO, up to 0.1 g/km for HC and up to 0.06 g/km for NO_x. Another type of emissions which are very hazardous for human health is soot and particulate formation. The Euro 6 standard limits these emissions to 6.0×10^{11} #/km for spark ignition (SI) and compression ignition (CI) engines [4]. Heavy duty (HD) vehicles are also regulated by EU emission standards and the limitations are becoming stricter. For example, one of the main targets for HD vehicles is to reduce CO_2 emissions by 15% in 2025 and by 30% in 2030 relative to 2019 and 2020 baseline data [5].

Strict regulations for exhaust gas emissions and the need to improve ICE efficiency have prompted a worldwide search for alternatives, such as transport electrification, hybridization and alternative fuels. It has been stated that by 2025, about 1 million public recharging and refueling stations will have to be afforded by EU state members for 13 million zero or low emission vehicles [6]. The EU has a target of

* Corresponding authors.
E-mail addresses: melaika@chalmers.se (M. Melaika), gilles.herbillon@gdtech.eu (G. Herbillon), dallas@chalmers.se (P. Dahlander).

https://doi.org/10.1016/j.fuel.2021.120454
Received 26 October 2020; Received in revised form 15 January 2021; Accepted 5 February 2021
Available online 27 February 2021

Nomenclature

A/F	air/fuel ratio
aTDC	after top dead center
bTDC	before top dead center
CA10-90	crank angle degrees between 10% and 90% of burned fuel
CAD	crank angle degree
CNG	compressed natural gas
CoV	coefficient of variance
CR	compression ratio
DI	direct injection
E10	gasoline with 10% ethanol addition
GDI	gasoline direct injection
H_2	hydrogen
HD	heavy duty
HC (THC)	Hydrocarbons (Total Hydrocarbons)
H:C	hydrogen and carbon ratio
ICE	internal combustion engine
IMEP	indicated mean effective pressure
iSFC	indicated specific fuel consumption
iSCO	indicated specific carbon monoxide emissions
$iSCO_2$	indicated specific carbon dioxide emissions
iSHC	indicated specific total hydrocarbon emissions
$iSNO_x$	indicated specific nitrous oxide emissions
ITE	indicated thermal efficiency
LD	light duty
LHV	lower heating value
LNG	liquified natural gas
MBT	maximum break torque
MFB50	50% of burned fuel mass
MN	methane number
PAH	polyaromatic hydrocarbons
PFI	port fuel injection
PM	particulate matter
PN	particulate number
PNC	particulate number concentration
RoHR	rate of heat release
rpm	revolutions per minute
SI	spark ignition
SOI	start of injection
ST	spark timing
VOCs	volatile organic compounds
WOT	wide open throttle
λ	lambda
η_i	indicated thermal efficiency
T_{exh}	exhaust gas temperature
p_{cyl}	cylinder pressure

achieving 20% electric vehicles (EVs), 40% hybrid electric vehicles (HEVs), 10% fuel cell electric vehicles (FCEVs) and 30% conventional vehicles by 2030, which would give an overall 70% reduction of CO_2 emissions from passenger cars [7]. However, ICEs and HEVs still form a major part of the powertrains market. Thus, improvements in ICE efficiency and exhaust emissions remain very important. Also, the combination of an electric powertrain and ICE in HEVs and mild hybrid electric vehicles (MHEVs) allow ICE operate in a better efficiency area and use an engine as range extender (in steady-state operation). Previous studies have investigated not only gasoline ICEs in HEVs but also other fuel types as alternatives. Experimental results have revealed that plug-in hybrid electric vehicles (PHEVs) running on ethanol/gasoline mixtures can reduce CO_2 emissions by up to 52 g/km [8]. HD diesel vehicles have been investigated with hybrid MHEV technology utilizing a 30 kW electric motor [9]. From 2 to 3 L of fuel per 100 km were saved during a typical city driving cycle. Gaseous fuel, i.e., compressed natural gas (CNG), has been investigated in a MHEV system (15 kW EM) and shown to give ~7% fuel savings compared to a conventional vehicle [10]. A hydrogen fueled ICE in a HEV has also been investigated and shown to offer benefits of reduced emissions and fuel consumption [11]. Previous studies have demonstrated that compared to gasoline, diesel and ethanol, CNG fuel gave the highest benefits in terms of reducing fuel consumption and CO_2 emissions in combination with a 48 V MHEV system in different driving cycles [12]. The benefits of natural gas or biomethane are mainly due to their chemical composition.

Methane-based fuels, e.g., natural gas and biomethane, are particularly promising as an alternative fuel because the main component methane (CH_4) has a higher H:C ratio than other fuels. A lower number of carbon atoms in the fuel composition leads to lower formation of CO_2, CO and hydrocarbons [13,14]. Other advantages of methane are it is in the gaseous phase and can easily be mixed with other gases, e.g., hydrogen (H_2), which can further improve exhaust gas emission levels. Also, CNG fuel can be mixed with the cleaned final biogas product biomethane, which can reduce well-to-wheel CO_2 emissions [15,16]. Natural gas has a higher octane number and is more resistant to knock phenomena than conventional fuels. Thus, higher engine compression ratios (CRs) can be applied. Engine tests with high CRs have shown that with CNG, the engine efficiency can be improved, lean limits extended, and HC and CO emissions decreased [17]. Additional positive effects were observed upon H_2 addition to the CNG mixture.

However, CNG fuel also has several drawbacks which influence the engine performance. Compared to gasoline, natural gas has a lower burning rate, higher quenching distance and narrow flammability range. Also, it requires a higher ignition energy [18]. Another issue is related to the engine maximum power output. Current CNG vehicles are equipped with a port fuel injection (PFI) system and natural gas is injected into the air intake manifold. The injected gas occupies a larger volume and reduces the engine volumetric efficiency, which affects the maximum power output [19]. Recently, companies have developed downsized turbocharged SI PFI CNG engines with high CR (CR = 13.3:1) which can reach the same performance as a downsized gasoline direct injection (GDI) engine [20]. However, newly designed downsized and heavily turbocharged engines can have substantially increased manufacturing costs [21].

One way to improve the engine volumetric efficiency, achieve a higher engine performance and improve exhaust gas emissions with CNG is to apply a gaseous fuel direct injection (DI) system. One of the studies has shown that DI-CNG can achieve up to 30% fuel savings compared to a GDI system [22]. Experimental results have shown that DI-CNG provides benefits at low load conditions compared to PFI since the combustion duration is longer for PFI [23]. The experiments also showed that DI achieves a higher indicated thermal efficiency (ITE) than PFI at lean conditions. It was suggested that the most critical issue for improving ITE in PFI under lean conditions is the combustion speed (the duration between the spark ignition and MFB50) [23]. Furthermore, it was stated that a late high pressure (100 bar) injection strategy for a DI-CNG system can increase the power output because of an increased volumetric efficiency, which is opposite with early injection timings [24,25]. The benefits of DI-CNG have also been observed in exhaust gas emissions. Hofmann et al. have shown that HC emissions can be drastically reduced with a DI-CNG system [22]. The increased engine load decreased the mass fuel burned fraction (50%) (MFB50) and total hydrocarbons (THC) due to enhanced intake air flow motion and a larger amount of the air/fuel mixture [23]. Also, CO emissions were drastically reduced with the DI-CNG system [22]. Tests have shown that CO_2 emissions from DI-CNG were lower than in gasoline PFI cases [26].

However, other researchers have noted that some standard emissions, e.g., hydrocarbons, were increased with a gaseous DI system compared to PFI and were mainly influenced by the start of injection timing (SOI) [23,26]. Later injection timings with a DI-CNG system increased cycle-to-cycle combustion variations and HC emissions [27]. The composition of CNG fuel also had an impact on standard emissions and soot formation when a DI system was applied [28].

An understanding of soot emissions formation from a CNG engine is also very important. Studies have suggested that CNG fuel offers a high potential for lowering soot emissions. Particulate measurements have shown that natural gas engines can deliver soot free combustion. It is claimed that natural gas engines can achieve near zero mass of particulate matter (PM) [29]. Tests with a DI-CNG 16 bar injector have shown that particle number (PN) emissions with a DI-CNG system were at a non-critical level [22]. It has been reported that the PN from a CNG HD vehicle is mainly due to nucleation mode particles originating from combusted engine lubrication oil [30,29]. Nanoparticles below 25 nm in diameter have been shown to dominate the physical composition in natural gas engines [31]. However, other experimental studies have shown that using a PFI-CNG system in a HD SI engine under WLTC driving conditions generates a higher peak of accumulation mode particles of ~ 100 nm diameter, with the peak reaching more than 5×10^6 particles/cm^3 [32]. Comparison of diesel, gasoline, CNG, CNG/H_2 mixture and H_2 fuels showed that diesel emitted the highest PN among all the fuels. As expected, lower PN levels were achieved with all the gaseous fuels. However, at specific engine load points, gasoline achieved slightly lower nucleation and accumulation mode particle levels than CNG fuel (PFI system) [33].

It is clear that ICE technology will be present for a long time in the ground transportation sector. Therefore, it is important to investigate different alternative fuel injection strategies in order to achieve a higher engine efficiency and reduce hazardous exhaust gas emission levels. One of the most promising alternative technologies is DI-CNG. Recent studies have revealed that it is important to continue the development of DI-CNG technology and improve our understanding of its effects on engine performance.

The present study included an experimental investigation of a single cylinder SI engine with GDI, PFI-CNG or DI-CNG systems and the same engine layout. The main focus was to compare liquid (gasoline) and gaseous fuel (natural gas) in a SI naturally aspirated engine based on an engine work map area covering most engine working points from low (1500 rpm) to high engine speed (2500 rpm) and from low to high load conditions. The aim was to investigate and explain how a gaseous fuel helps to improve the SI engine efficiency and reduce standard emissions and soot reduction, as well as how the DI-CNG spray guided system provides additional benefits compared with standard vehicle fuel systems, i.e., GDI spray guided and PFI-CNG.

2. Experimental setup

Experiments were conducted using an AVL engine test bench with a single cylinder SI engine equipped with a 4 valve system cylinder head. Engine technical specifications are presented in Table 1.

Table 1
Engine specifications.

Parameter	Value
Displaced volume (V_h), [dm^3]	0.5
Stroke (S), [mm]	90.0
Bore (D), [mm]	82.0
Connecting rod (L_{conr}), [mm]	139.5
Compression ratio (CR), [-]	10:1
Number of valves, [-]	4
Intake air temperature (T_{air}), [°C]	+25
Intake valve opening (IVO), [CAD]	356
Intake valve closing (IVC), [CAD]	578
Exhaust valve opening (EVO), [CAD]	145
Exhaust valve closing (EVC), [CAD]	357

The engine had a compression ratio (CR) of 10:1, which was also suitable for air turbocharger modification. The whole experimental campaign used a single electrode spark plug with the same electrode positioning in the cylinder. The intake and exhaust valves had a few crank angle degrees (CADs) overlap.

A schematic of the engine setup is presented in Fig. 1. The engine was supplied with an external air supply system to maintain a stable air flow, air pressure and temperature supply to the engine, ensuring test data stability and avoiding the influence of additional parameters fluctuations on the engine work process.

The air intake temperature was kept constant at + 25 °C during the whole experimental campaign. The air supply pressure to the engine was kept constant at 1 bar. The air intake pressure was regulated according to the required amount for the combustion to keep the air/fuel (A/F) mixture at stoichiometric ($\lambda = 1.0$) conditions. The air flow and air pressure in the air intake manifold were controlled by the throttle valve. The air intake ports were equipped with air pressure and temperature sensors to monitor and ensure a closed loop control system.

Technical data for the tested solenoid type Denso GDI injector are listed in Table 2. The injector was mounted in the same position in the cylinder head as for DI-CNG system. Gasoline fuel was supplied through the Coriolis mass flow meter to the injector. The fuel was injected via a 6-hole injector nozzle. GDI cases were tested with a 200 bar injection pressure, which is a standard pressure used in current LD GDI SI engines.

The PFI-CNG system was mounted in the air intake manifold with a Landi Renzo GIRS12 solenoid type injector positioned upstream in the intake runner. The injector's technical characteristics are also listed in Table 2. The PFI-CNG injector injected fuel into two fuel supply lines (Fig. 1). Two separate fuel injection lines were connected on the intake runner on opposite sides to each other to promote better gaseous fuel mixing with air in the air intake runner. The CNG fuel was supplied from a pressurized 200 bar bottle. The gas pressure was reduced to 18 bar pressure and supplied to the same type Micro Motion Elite Coriolis mass flow meter. After the gas flow measurement system, the gas was directed to a gas reducer, which was able to reduce the gas pressure down to a 1–4.5 bar. Gas at reduced pressure was supplied to the PFI injector.

Prototype DI-CNG injector tests were conducted with a solenoid type injector mounted into the top of the cylinder head (Fig. 2). The GDTech DI-CNG injector's specifications are also presented in Table 2. Gas was injected through a 10-hole injector nozzle. The holes were directed in various symmetric directions to the cylinder axis. The injection pressure varied with the engine load. Different injection pressure strategy was selected considering the injector limitations, injection process physics, required fuel mass to achieve desired engine load and combustion stability. An injection pressure of 18 bar was used at low indicated mean effective pressure (IMEP) (4.5 bar) and mid (6 bar) load points.

An injection pressure of 50 bar was used for high (9 bar IMEP) engine load points. Such an injection pressure strategy ensured that the injection duration was sufficiently short to inject required high fuel mass (compared to low load points) in a short period of time but avoiding too short injections where nonlinear injection can appear. Nonlinear injections can cause high shot-to-shot variations, resulting in high combustion cycle-to-cycle variations. Use of a high injection pressure (50 bar) ensured sufficiently shorter injection durations when a high amount of fuel needed to be injected and the injection duration could not be prolonged too much because of time limits, especially at high engine speeds. The requirement of different injection pressures for different engine operating points were also discussed by [34] where it was stated that at idle or low load conditions injection duration should be prolonged by lower injection pressure and at higher loads the injection pressure should be higher.

The CNG fuel to DI-CNG injector was supplied in the same way as for the PFI case and the injection pressure was again controlled with a pressure regulator mounted at the start of the fuel supply line, at the gas

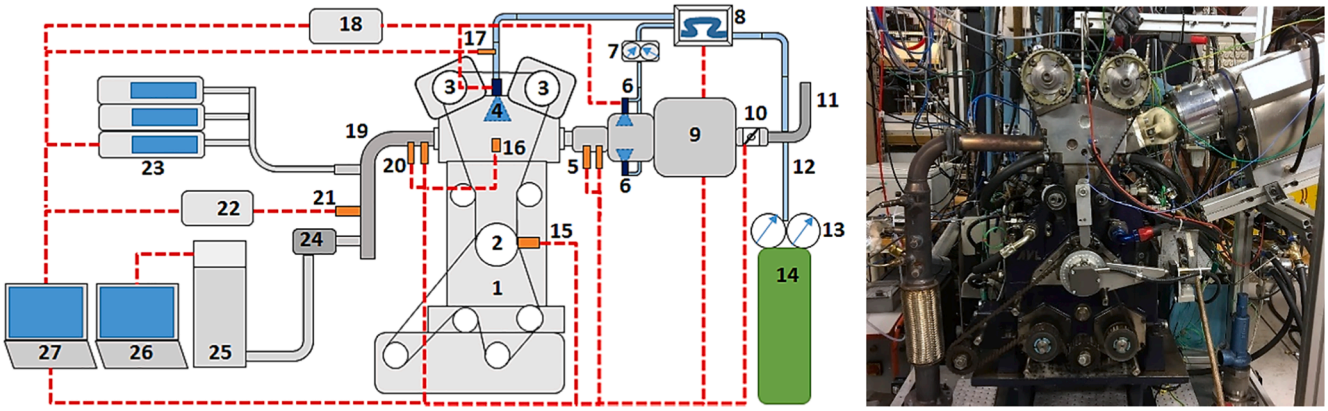

Fig. 1. Test engine system layout: 1 – AVL single cylinder SI engine; 2 – crankshaft; 3 – camshafts; 4 – GDTech DI-CNG injector; 5 – intake air pressure and temperature sensors; 6 – Landi Renzo GIRS12 PFI-CNG injectors rail; 7 – Landi Renzo two stage gas pressure reducer for PFI system; 8 – Micro Motion Elite Coriolis fuel flow meter; 9 – air intake plenum and runners; 10 – throttle valve; 11 – compressed air supply system; 12 – fuel supply line; 13 – gas pressure regulator; 14 – CNG tank; 15 – AVL 365 crank angle encoder; 16 – AVL GH14DK cylinder pressure sensor; 17 – Kistler 4618A2 gaseous fuel pressure sensor in fuel supply line; 18 – NI Direct Injector Drive System for DI and PFI injector control system; 19 – exhaust gas pipe; 20 – exhaust gas pressure and temperature sensors; 21 – lambda sensor; 22 – Horiba Mexa-110 A/F ratio measurement system; 23 – standard emissions analyzers J.U.M. VE7, Fuji Electric ZPA, Eco Physics CLD822 CMhr; 24 – heated sample line for fast particulate analyzer; 25 – Cambustion DMS500 MkII fast particulate analyzer; 26 – fast particulate analyzer data sampling computer; 27 – AVL Indicom and AVL Puma software for engine control and data acquisition.

Table 2
Tested injection system specifications.

Injector type	GDI	PFI-CNG	DI-CNG
Injection position	Cylinder	Air intake manifold	Cylinder
Injector type	Solenoid	Solenoid	Solenoid
Control peak/hold, [V]	65/12	12	65/12
Injection pressure, [bar]	200	1–4.5	18–50
Injector nozzle	6 holes	1 hole	10 holes
Opening direction	Inwards	Outwards	Inwards

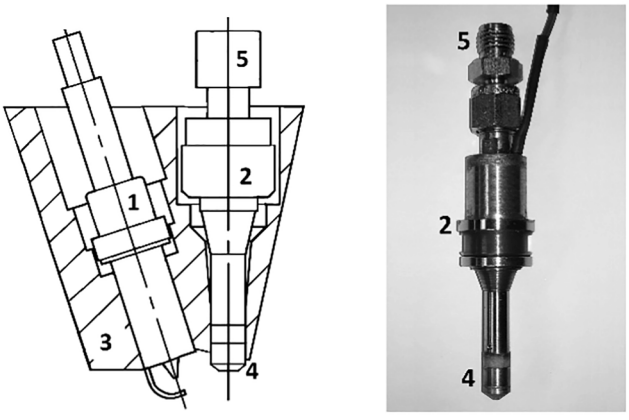

Fig. 2. Spray guided DI-CNG injector and schematic of injector positioning in the engine cylinder head: 1 – single electrode spark plug; 2 – centrally mounted DI-CNG injector; 3 – engine cylinder head; 4 – injector nozzle tip; 5 – gas connection to the injector.

bottle. A high speed pressure sensor (CAD resolved) Kistler 4618A2 was mounted as close as possible to the DI-CNG injector on the fuel supply pipe. Fuel pressure measurements enabled monitoring of the precise injection pressure, pressure drops and pressure fluctuations after each injection.

The GDI, PFI-CNG and DI-CNG injectors were controlled with a National Instruments Direct Drive System control module. The injected fuel mass was adjusted according to the Lambda sensor signal. The fuel mass was adjusted by the injection duration in milliseconds (ms) to achieve the required engine load and ensure stoichiometric conditions.

A 90% gasoline/10% ethanol fuel mixture (E10) was used for the GDI tests. The physicochemical properties of liquid fuel E10 are presented in Table 3. The fuel properties were determined by laboratory tests according to the ISO4259 standard [35]. The fuel had a H:C ratio of 1.91:1 with a lower heating value (LHV) of 42.79 MJ/kg. It comprised 13.4% hydrogen, 83.5% carbon and 3.14% of oxygen according to mass.

The properties of natural gas used for both the PFI-CNG and DI-CNG tests are presented in Table 3. The natural gas fuel was prepared by a gas production company and it mixed the CNG fuel according to a presented composition (Table 3). This ensured that the fuel composition was the same as that from the Swedish natural gas grid and petrol stations [36]. Also, it ensured that the fuel composition did not vary and eliminated the ability to influence other engine characteristics (emissions, power, efficiency, etc.) which depend on fuel combustion process. The CNG composition mainly consisted of methane CH_4 (88.8%) and some added higher hydrocarbons, e.g., ethane C_2H_6, propane C_3H_8 and butane C_4H_{10}. It is known that addition of these hydrocarbons can improve the natural gas combustion. The CNG also had a small percentage of nitrogen (N_2) and carbon dioxide (CO_2) diluents in its composition. The Swedish gas market currently blends biomethane with natural gas in the grid. This results in small amounts of the mentioned diluents in the total gas composition. The presence of N_2 and CO_2 in the composition can have a negative impact on the combustion because they can slightly

Table 3
Physicochemical properties of the gasoline fuel (E10) and natural gas.

Properties	Gasoline E10	CNG
Fuel composition, [$\%_{Vol.}$]	Gasoline 90%	CH_4 88.8% ± 1.80% C_2H_6 6.0% ± 0.12% C_3H_8 2.5% ± 0.05%
	Ethanol 10%	C_4H_{10} 0.6% ± 0.01% N_2 0.7% ± 0.04% CO_2 1.4% ± 0.03%
Hydrogen (H) %	13.37	23.89
Carbon (C) %	83.51	76.11
Oxygen (O) %	3.14	–
H:C ratio	1.91:1	3.72:1
Density at + 15 °C, [kg/m^3]	757	0.776
Octane number (RON)	95.3	
Octane number (MON)	85.2	–
Methane number (MN)	–	74
Stoichiometric A/F ratio, [kg_{air}/kg_{fuel}]	14.65	16.95
Lower heating value, [MJ/kg]	42.79	47.27

reduce RoHR during the combustion. However, the gaseous fuel had a higher hydrogen and lower carbon percentage according to the mass compared to a gasoline fuel in the total fuel composition. This resulted in a higher H:C ratio for natural gas (H:C = 3.72:1), which was almost two times higher than the gasoline fuel (H:C = 1.91:1). Hence, for CNG, the formation of carbon-based exhaust gas emissions, e.g., carbon monoxide (CO) and carbon dioxide (CO_2), and even hydrocarbons were expected to be lower. The lower carbon content was also expected to result in lower PN formation. The LHV was also higher for CNG (47.27 MJ/kg), indicating that a larger amount of energy was available for the same mass. However, the density of the gaseous fuel (0.776 kg/m^3) was considerably lower than for the liquid fuel. This can cause issues related to the CNG fuel energy amount based on volume. In particular, the gas occupied more volume when injected into the engine cylinder, reducing the engine's volumetric efficiency. On the other hand, the CNG fuel had a higher octane number compared to gasoline, making it highly resistant to knock. The CNG fuel also had a methane number (MN) of 74, which meets the SS-EN16723-2:2017 Swedish and European standard for natural gas and biomethane use in transport as an automotive fuel [37].

As mentioned above, different engine load points were tested at stoichiometric conditions. The stoichiometric conditions were determined by measuring the oxygen content with a lambda sensor in the exhaust gases. A Horiba Mexa-110 system was used to determine the air/fuel (A/F) ratio (measurement ranges and accuracy are given in Table 4).

The engine cylinder pressure was measured with an AVL GH14DK pressure sensor (sensor sensitivity 19 pC/bar) (Table 4) to investigate the combustion process and calculate the rate of heat release (RoHR). All pressure data were sampled using an AVL Indicom data acquisition system. Data for the cylinder pressure and RoHR were postprocessed using a MATLAB.

Liquid gasoline fuel and gaseous CNG fuel were measured with Micro Motion Elite Coriolis mass flow meter (CMF010M323NB). The fuel mass flow meter measurement range and accuracy are also presented in Table 4.

The exhaust gas composition was measured with standard emission analyzers (Fig. 2). Total hydrocarbons (THC) was measured with a J.U. M. VE7 flame ionization detector (FID). CO_2 and CO were measured by the non-dispersive infrared method (NDIR) with a Fuji Electric ZPA gas analyzer. NO_x emissions were measured with Eco Physics CLD822 CMhr equipment based on a chemiluminescence method. The exhaust gas sampling line was kept at + 190 °C to avoid gas condensation. The equipment measurement ranges and accuracy values are presented in Table 4. A Cambustion DMS500 MkII fast particle analyzer was used to measure the particle size distribution and PN in the exhaust gases. A dilution system comprising primary and secondary diluters was used. The dilution factors were adjusted for gasoline and natural gas to keep the signal strength within required limits. The diluted gas flow was compensated by the analyzer software. The sampling probe was connected to the exhaust gas pipe separately from the standard exhaust gas analyzers (Fig. 1). The primary diluter and whole sampling line were heated up to + 150 °C (according to measurement equipment requirements) to avoid condensation in the sampling line. Use of an even temperature over the sampling line helped to reduce losses due to temperature gradients. PN measurement ranges and accuracies of the PN measurement equipment are presented in Table 4.

Table 4
Measurement ranges and errors for the directly measured data.

Parameter	Measurement range	Error
Torque (T), [Nm]	–	±0.10%
Lambda (λ)	0.5–2.5	±0.70%
Cylinder pressure (p_{cyl}),[bar]	0–300	±1.50%
Fuel flow (m_f), [kg/h]	0.96–45.0	±0.35%
THC, [ppm]	0–1000	±1.00%
CO, [%]	0–5	±0.50%
CO_2, [%]	0–25	±0.50%
NO_X, [%]	0–5000	±1.00%
PN, [nm]	5–300	±5.00%
	300–1000	<10.0%

3. Experimental methodology

The experimental campaign test points are listed in Table 5. Tests included three different fuel injection systems – GDI, PFI-CNG and DI-CNG.

The fuel injection systems were tested at three engine speeds (1500, 2000 and 2500 rpm) and three engine loads (4.5, 6 and 9 bar IMEP) to cover a minimized engine work map. All operated engine points were carried out at stoichiometric conditions ($\lambda = 1.0$). The minimized engine work map covered the most relevant engine regimes of a vehicle under real driving conditions. It was determined in previous studies that similar displacement engine is used most of the time at these engine operating points while running the NEDC, WLTC or RTS95 driving cycles [38]. Engine maps of different parameters were postprocessed and presented as surface plots using MODDE and MATLAB software. Intermediate points between tested points were interpolated according to directly measured or calculated values with the highest significance for the model as possible. Interpolated values are presented as isolines in the maps. All engine parameters maps are displayed with R^2 values, which show how well the model fitted the data. Some of the map plots include values in rectangles, which represent the difference (in percentage) of measured values at tested points compared to the GDI case. The R^2 values are not related to the mentioned calculated percentages. Model fitting values (R^2) were calculated based on directly measured or calculated values at 9 tested points for the three fuel injection systems.

All three fuel systems achieved the targeted 4.5 and 6 bar IMEP bar load (Table 5). However, differences appeared at 9 bar IMEP. The PFI-CNG and DI-CNG tests showed that the highest engine load point was achieved just with a wide-open throttle (WOT). Some test cases (PFI-CNG at 2000 rpm, DI-CNG at 1500 rpm and 2000 rpm) showed that the maximum engine load was slightly below the targeted 9 bar IMEP. A lower maximum IMEP can be explained by a reduced volumetric efficiency, as described in the Introduction and explained further in the Results and Discussion.

Injection timings were chosen from a trade-off between high combustion stability, low particulate and standard emissions. The SOI timing for GDI was 310 CAD bTDC. The injection timing for DI-CNG was the same as for the gasoline cases. The same early 310 CAD bTDC timing unified the testing points so that the results could be compared in a fair way. It is known that CNG can reduce engine volumetric efficiency and late injection timings would improve it. However, late injection timings in DI-CNG system has another drawback – THC emissions increase due to insufficient time for air and fuel mixing, less homogeneous mixture achieved [39]. PFI-CNG used a slightly earlier SOI at 330 CAD bTDC.

Spark timings were individually adjusted for each testing point (Table 5). The spark timings were selected to reach a combustion phasing MFB50 at 6–8 CAD aTDC. This also resulted in low coefficient of variance of IMEP (CoV_{IMEP}) for all tested cases. Due to differences in flame propagation speed between gasoline and CNG fuel the values of spark timings show that PFI-CNG required slightly earlier ignition at low/mid load points in 1500–2000 rpm range. DI-CNG combustion required few degrees later spark timing compared to PFI-CNG showing that DI system for gaseous fuel had an impact on combustion process which will be later discussed in the results chapter. Most of the high engine load points with PFI-CNG and DI-CNG required same or later spark timing as for GDI. The main reason behind that is that CNG high load cases were tested at WOT conditions and high load operating points for GDI were reached with slight throttling.

Pressure data measurements consisted of 300 combustion cycles measured continuously during one test run. Tests of each engine load point at different engine speeds were repeated at least 5 times, meaning

Table 5
Operated engine points with different fuel injection systems.

	Engine speed (N), [rpm]	Engine load (IMEP), [bar]	Lambda, -	Injection timing (SOI), CAD bTDC	Spark timing (ST), CAD bTDC	Air intake pressure (p_{int}), [bar]
GDI	1500	4.54			20	0.590
		6.04	1.0	310	17	0.705
		9.03			14	0.904
	2000	4.52			21	0.570
		6.02	1.0	310	19	0.690
		9.04			16	0.925
	2500	4.51			23	0.518
		5.99	1.0	310	19	0.630
		8.99			17	0.852
PFI-CNG	1500	4.52			22	0.642
		6.03	1.0	330	19	0.772
		9.03 (WOT)			14	1.000
	2000	4.52			22	0.632
		6.01	1.0	330	20	0.768
		8.62 (WOT)			17	1.000
	2500	4.52			22	0.589
		6.00	1.0	330	18	0.714
		9.47 (WOT)			16	1.000
DI-CNG	1500	4.54			22	0.644
		6.03	1.0	310	17	0.779
		8.89 (WOT)			16	1.000
	2000	4.52			21	0.631
		6.03	1.0	310	18	0.772
		8.42 (WOT)			18	1.000
	2500	4.52			19	0.588
		6.03	1.0	310	16	0.718
		9.39 (WOT)			17	1.000

that a total of at least ~ 1500 combustion cycles were analyzed for each map point. Exhaust gas emissions and fuel consumption were measured for at least 30 s in each point and averaged values were calculated from at least 5 repetitions. PN samples were taken for at least 2 min at a frequency of 5 Hz and 3 times for each engine load point, engine speed and repetition.

Important parameters were calculated using the measured data, e.g., RoHR, indicated specific fuel consumption (iSFC), indicated engine efficiency (η_i) and CoV_{IMEP}. The net rate of heat release was calculated according to [40]:

$$\frac{dQ_{net}}{d\theta} = \frac{\gamma}{\gamma - 1} p_{cyl} \frac{dV}{d\theta} + \frac{1}{\gamma - 1} V \frac{dp}{d\theta}; \quad (1)$$

where θ is the crank angle degree (CAD), γ is the specific heat ratio, p_{cyl} is the pressure in the cylinder and V is the cylinder volume at the specific CAD. Integration of Q_{net} as a function of θ gave the total released energy as the mass fraction burned (MFB). From 10% to 90% of released total energy indicated a combustion duration of CA10-90.

The indicated specific fuel consumption (iSFC) was calculated according to [40]:

$$iSFC = \frac{\dot{m}_f}{P_i}; \quad (2)$$

$$P_i = \frac{W_{c,i} \cdot N}{n_r}; \quad (3)$$

where $\dot{m}_f$ is the fuel mass flow rate per unit time, P_i is the indicated engine power, $W_{c,i}$ is the indicated work per cycle calculated by integrating the p-V curve ($W_{c,i} = \int pdV$), N is crankshaft rotational speed, n_r is the the number of crank revolutions for each power stroke per cylinder. The engine indicated efficiency (η_i) was also calculated according to [40]:

$$\eta_i = \frac{1}{iSFC \cdot Q_{LHV}}; \quad (4)$$

where Q_{LHV} is the fuel lower heating value. The values of CoV_{IMEP} were obtained from [40]:

$$CoV_{IMEP} = \frac{\sigma_{IMEP}}{\overline{IMEP}}; \quad (5)$$

where σ_{IMEP} is the standard deviation of IMEP and $\overline{IMEP}$ is the mean value of the indicated mean effective pressure.

Table 6 shows the standard uncertainties for indirect measurements like IMEP, η_i, iSFC and indicated specific standard emissions (iSHC, $iSCO_2$, iSCO, $iSNO_x$).

The standard uncertainty $u_c(y)$ characterizes the dispersion of the values that can reasonably be attributed to the measurand $Y = f(X_1, X_2, \cdots, X_N)$, where Y is not measured directly and determined from N other quantities X_1, X_2, …, X_N through a functional relationship f. Indirect measurement combined standard uncertainties $u_c(y)$ were determined from the estimated standard deviation associated with each input estimate x_i, which was termed the standard uncertainty $u(x_i)$ according to the ISO/IEC standard [41]:

$$u_c^2(y) = \sum_{i=1}^{N} \left(\frac{\partial f}{\partial x_i} \right)^2 u^2(x_i); \quad (6)$$

where u is the standard uncertainty evaluated statistically from repeated observations and $u_c(y)$ is the combined standard uncertainty, which is an estimated standard deviation associated with the output estimate or measurement result y.

Calculation of the combined uncertainties showed that the variations of indirect measurement values in the presented engine maps were from

Table 6
Calculated indirect measurement standard uncertainties.

Parameter	Uncertainty
IMEP, [bar]	±1.00%
η_i, [-]	±1.25%
iSFC, [g/kWh]	±2.07%
iSHC, [g/kWh]	±2.48%
iSCO, [g/kWh]	±1.35%
$iSCO_2$, [g/kWh]	±1.71%
$iSNO_X$, [g/kWh]	±1.97%

± 1.00% for IMEP to ± 2.5% for iSHC values.

4. Results and discussions

4.1. Engine efficiency, combustion and indicated parameters

The analysis of engine efficiency and combustion parameters are mainly presented as engine map figures for GDI, PFI-CNG and DI-CNG system tests. As mentioned before, tests were conducted at different engine loads and engine speeds. The maps include data values at engine loads from 4.5 bar IMEP to ~ 9.5 bar IMEP and engine speeds from 1500 rpm to 2500 rpm. The maps include isolines showing the trends in measured values with the values labeled on the isolines. Blue points show the tested engine points. Some of the map plots include values in a blue color in rectangles, which represent the difference (in percentage) of measured values at tested points compared to the GDI case.

An initial investigation of the cylinder pressure and heat release curves was conducted to obtain a better understanding of how the different fuel systems influenced the combustion process. Curves for the GDI, PFI-CNG and DI-CNG systems are presented in Fig. 3 for the three tested engine loads 4.5 bar, 6 bar and 9 bar IMEP at the same engine speed of 2000 rpm. Other engine speed points were recorded but are not presented in this paper as the trends were similar to the curves in Fig. 3.

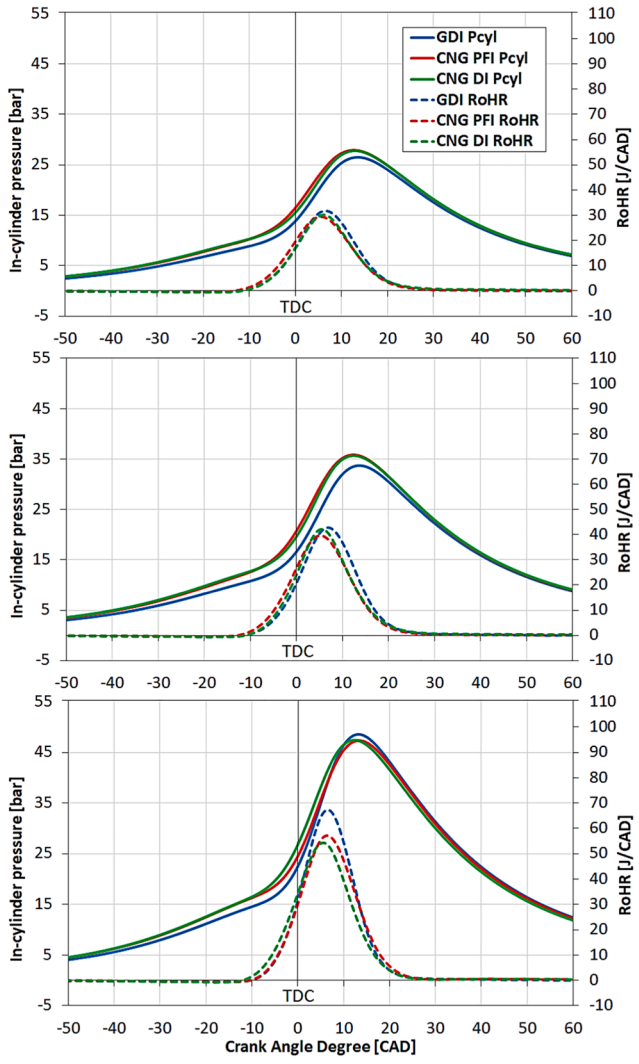

Fig. 3. Cycle averaged cylinder pressures and RoHR comparison between GDI, PFI-CNG and DI-CNG at a) 4.5 bar, b) 6 bar and c) 9 bar IMEP and 2000 rpm engine speed.

Initial analysis of the cylinder pressure and RoHR showed that they increased with engine load, as expected. Cylinder peaks for all cases were determined at 12–13 CAD aTDC, which ensured that the MBT could be achieved. The graphs show that the PFI-CNG and DI cases had the highest maximum cylinder peaks, which were higher by a few bars compared to GDI. The peak increase for the gaseous fuels was mainly attributed to a higher intake air pressure. The data in Table 5 show that the air intake pressures for PFI-CNG and DI-CNG were higher compared to those for GDI. As mentioned before, the engine's volumetric efficiency decreases with gaseous fuels. This is because gaseous fuels occupy a larger volume in the cylinder, reducing the volume available for air. To compensate for this, the throttle had to be opened more and more air had to be supplied to achieve the same engine load level as for GDI case.

Heat release plots showed that a higher energy content was released in the GDI cases. Spark timing data (Table 5) and calculations of RoHR indicated that the gaseous fuel combustion process was different from those of the liquid fuel cases. The CNG gas had a longer combustion and RoHR values were lower compared to the gasoline fuel. The spark timing in the gaseous fuel cases had to be advanced to achieve the MBT when CA50 was at 6–8 CAD aTDC because natural gas had a longer and slower combustion than gasoline. However, RoHR showed that the combustion was different between the PFI and DI systems with natural gas fuel and varied slightly depending on engine load.

The combustion RoHR was lower for PFI-CNG at the low load (4.5 bar IMEP) (Fig. 3a) and mid load (6 bar IMEP) point (Fig. 3b) than for DI-CNG. The slightly higher RoHR with DI-CNG may have been influenced by the fuel's direct injection, which improves fuel mixing with air and increases mixture motion in the cylinder due to turbulence. Higher turbulence in the cylinder increases the flame propagation speed and RoHR. These benefits of a DI system, i.e., improved mixture motion and turbulence, have also been observed by other researchers. Sankesh et al. reported that DI-CNG injection after intake valve closure at part loads increased the combustion rate [24]. Moon et al. discussed that the intake air flow motion and smaller amount of combustible mixture at low loads and lower air intake pressures showed a longer MFB50 and DI-CNG provided additional turbulence energy inside the cylinder [23]. Other researchers have reported that induced turbulence by the fuel jet is the main factor that increases turbulence and affects the flame propagation speed. A higher flame propagation speed has been shown to increase RoHR and the cylinder pressure [42].

An opposite trend was observed in the present study at the highest engine load (9 bar IMEP) (Fig. 3 c). DI-CNG achieved slightly lower RoHR than PFI-CNG. The decreased RoHR with the DI-CNG system may be explained by changes in gas exchange behavior at a certain engine speed. The IMEP values in Table 5 shows that PFI-CNG and DI-CNG cases achieved the lowest maximum load at WOT conditions at 2000 rpm compared to 2500 rpm. The issue related with gas exchange pulses and increased residuals were addressed in a previous study of the same engine configuration [43].

To understand the combustion stability behavior, we analyzed CoV_{IMEP} maps for the three tested fuel injection systems (Fig. 4).

The maps were constructed by polynomial interpolation of points between the three engine loads (4.5, 6, 9 bar IMEP) and different engine speeds (1500, 2000 and 2500 rpm). All the tested cases were conducted at the MBT timing (CA50-6-8 CAD aTDC). Stable combustion could be achieved for all fuels in all conditions. The GDI test cases showed (Fig. 4 a) that CoV_{IMEP} was always below 1% and varied from 0.52% to 0.96% at low and high engine load, respectively. As mentioned before, CoV_{IMEP} is an important factor for maintaining an adequate engine work process and a vehicle's drivability [40,44].

The combustion stability for both PFI-CNG and DI-CNG were slightly lower compared to GDI. PFI-CNG tests showed (Fig. 4b) that the lowest CoV_{IMEP} was ~ 0.91% at 2500 rpm and the highest load point (~9 bar IMEP). The highest variation of IMEP (2.3 to 3%) was at the lowest load point 4.5 bar IMEP for all engine speeds. A higher CoV_{IMEP} could be due to several reasons. The CNG flame speed is lower and the combustion

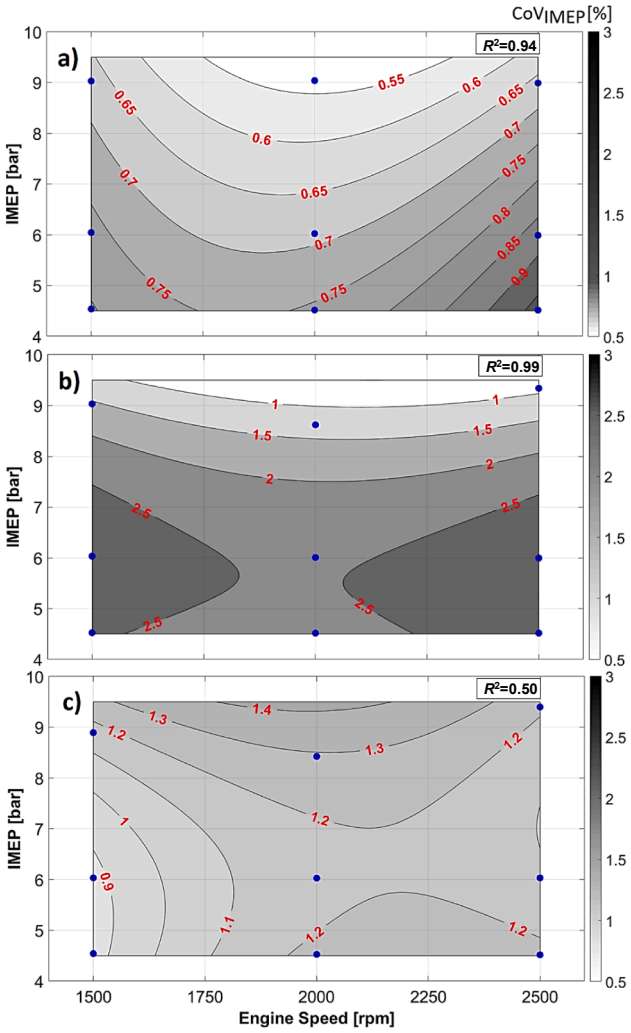

Fig. 4. Combustion stability CoV_{IMEP} (%) comparison between a) GDI, b) PFI-CNG and c) DI-CNG at different engine speeds and loads.

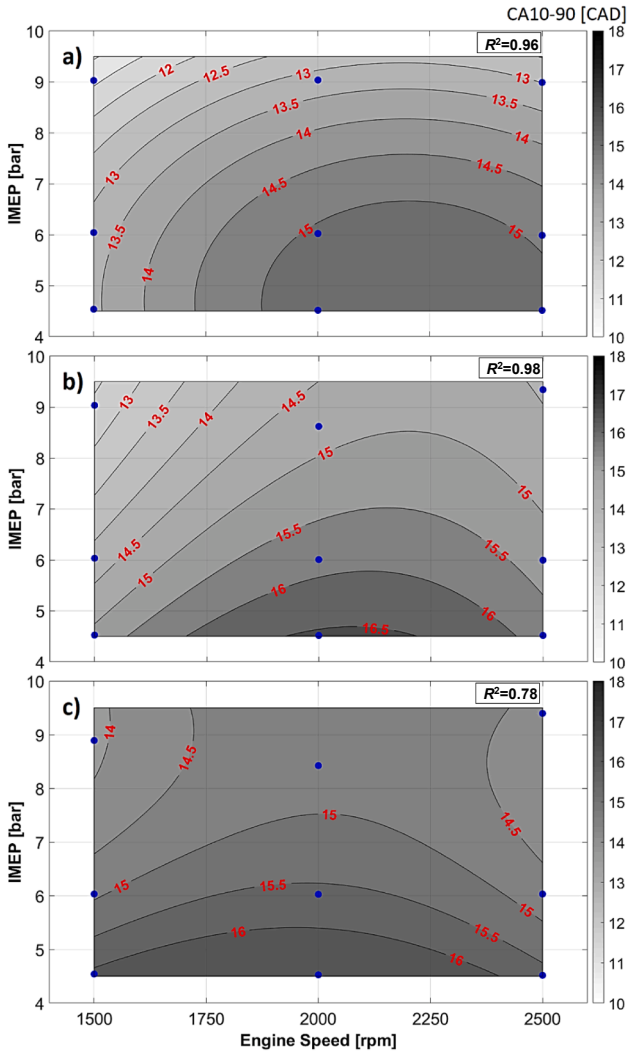

Fig. 5. CA10-90 (CAD) comparison between a) GDI, b) PFI-CNG and c) DI-CNG at different engine speeds and loads.

temperature is also lower compared to gasoline fuel. Decreased combustion stability with PFI-CNG system at lower engine load was discussed by [45]. It stated that at higher engine loads higher combustion temperature was achieved compared to low load conditions. Increased combustion temperature enhances the chemical reactivity which increase the combustion stability. The mixing issues of the CNG fuel with air may also have caused increased variations in IMEP. The injected fuel mass at low load points was smaller. Therefore, the combustion process was likely slower due to a lower energy content. DI-CNG tests showed (Fig. 4c) that CoV_{IMEP} was better than with PFI-CNG. CoV_{IMEP} values for the gaseous DI system were similar to those of the GDI cases, with CoV_{IMEP} never exceeding 1.5%. Mainly it varied from 0.95% up to 1.4%. The DI-CNG system was able to achieve very stable combustion in the low load map area at all engine speeds. Thus, the DI-CNG injector achieved more stable injections and less shot-to-shot variations between cycles at low injection pressure (18 bar) and low and mid load points or high injection pressure (50 bar) and high load points.

Surface maps of the combustion duration CA10-90 (Fig. 5) supported the engine cylinder pressure and RoHR data showing that GDI (Fig. 5a) had a shorter combustion duration by a few CADs than PFI-CNG (Fig. 5b) and DI-CNG (Fig. 5c) combustion in the whole map area. As mentioned before, DI-CNG showed an improved RoHR compared to the PFI-CNG system. CA10-90 for DI-CNG was slightly shorter at 2000–2500 rpm in the map area from mid (6 bar IMEP) to high engine load points (~9 bar IMEP) compared to the PFI data.

Fig. 6 shows a comparison of the engine indicated efficiency (η_i) for the three injection systems depending on load and engine speed. The GDI cases (Fig. 6a) showed that η_i increased from 0.32 to 0.33 at low load to 0.345–0.35 at high load points according to the engine speed. As expected, the highest indicated efficiency for GDI case was observed at the highest load points 9–9.5 bar IMEP. Engine thermal efficiency can be increased by increasing the air pressure and intake flow motion. This also helps to achieve a more complete combustion and decrease the duration between the spark ignition and MFB50 [23]. The η_i and CoV_{IMEP} surface map trends were consistent with each other.

The engine efficiency was the highest in the map areas where the combustion was the most stable. Similar trends were observed for the gaseous fuel cases.

The efficiency map for PFI-CNG (Fig. 6b) showed that the engine achieved from 3% to 4% higher η_i compared to the GDI tests. The highest η_i values for PFI-CNG were achieved at similar points as those for GDI, i.e., 2000 rpm, ~9 to 9.5 bar IMEP. The higher η_i for the PFI-CNG case was attributed to the CNG fuel properties. Natural gas has a higher LHV (47.27 MJ/kg) than gasoline (42.79 MJ/kg). Therefore, lower fuel consumption is required to achieve a similar engine load than in the GDI case. As mentioned in the Introduction, PFI-CNG systems usually have a disadvantage of lower volumetric efficiency, especially at low loads due to throttling. However, our study showed that a slightly higher engine

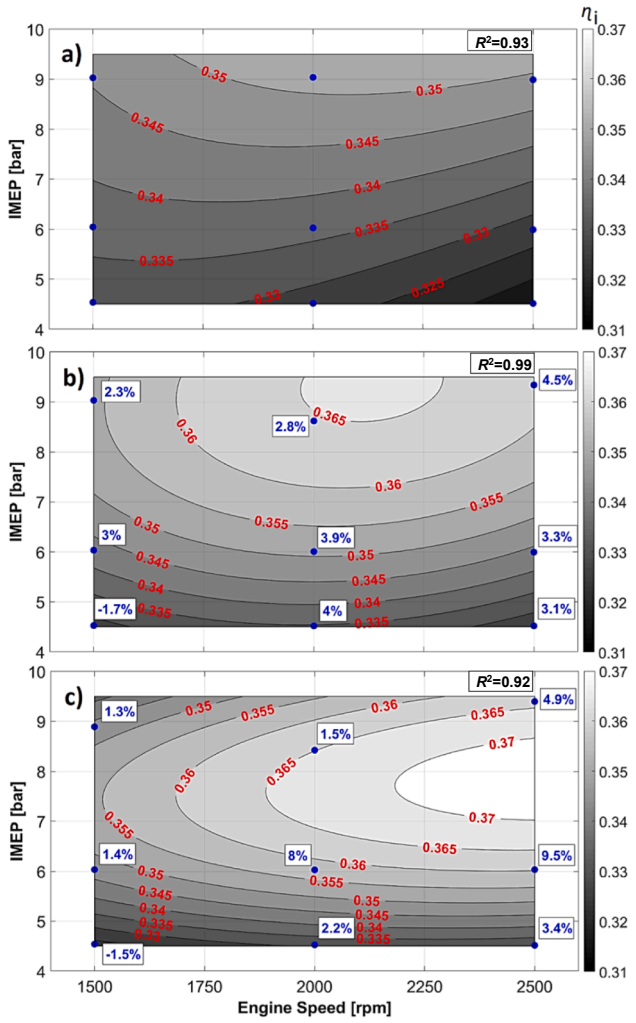

Fig. 6. Engine efficiency (η_i) comparison between a) GDI, b) PFI-CNG and c) DI-CNG at different engine speeds and loads.

efficiency was achieved for PFI-CNG than for GDI and the greatest benefit was observed at high load where the throttle was wide open. Similar trends were reported by Sevik et al. [46]. It also known that one of the main reasons of improved engine efficiency with PFI-CNG is related with the spark timing. CNG fuel has much higher-octane number, therefore the spark timing for the methane-based fuel can be advanced compared to gasoline. This was also discussed by [47] where higher octane number and early spark timing were the key parameters to improve the thermal efficiency and specific fuel consumption.

The surface map of engine η_i for the DI-CNG system (Fig. 6c) showed that the increase in efficiency could be even higher than for the GDI and PFI-CNG fuel systems. Similarly to PFI-CNG, DI-CNG achieved higher efficiencies for the SI engine than GDI. The improvement varied from 2% to 4% at high engine speeds (2000 to 2500 rpm) over a wide engine load range (from 4.5 bar to 9.5 bar IMEP). Noticeably, the most efficient map region for DI-CNG shifted toward higher engine speeds, i.e., ~2250 to 2500 rpm in the mid-high engine load area compared to GDI and PFI-CNG. The increase of η_i for DI-CNG was ~9% higher compared to GDI. This was attributed to better air/fuel mixing in the cylinder because of increased air motion at higher engine speeds and increased turbulence in the cylinder. This was supported by the combustion duration CA10-90 parameter map (Fig. 5c). In the same map region, the combustion duration was the shortest due to increased RoHR. The engine efficiency improvement with DI-CNG (Fig. 6c) in the mentioned map area was also influenced by a better volumetric efficiency compared to PFI-CNG as the gas was injected directly into the cylinder in the DI case.

As mentioned before, the most efficient map area for DI-CNG shifted to a higher engine speed point (from 2000 rpm to 2250–2500 rpm). The engine efficiency was lower for DI-CNG compared to PFI-CNG at 1500–2000 rpm engine speed and in the 9–9.5 bar load region. The η_i decrease was caused by slower and longer combustion, as confirmed by the RoHR calculations (Fig. 3c). CoV_{IMEP} for DI-CNG (Fig. 4c) was also higher at this engine test point compared to GDI (Fig. 4a) and PFI-CNG (Fig. 4b). This change in combustion process could be affected by air/fuel mixture inhomogeneities in the cylinder. Similar results have been observed by Moon et al., who showed that PFI-CNG achieved a higher thermal efficiency than DI-CNG because of better mixture homogeneity, which seems to be a critical factor for improving the efficiency at high engine load points [23].

The engine efficiency for DI-CNG at low engine speed (1500 rpm) and engine load (4.5 bar IMEP) was lower by 1.5% compared to GDI. A similar trend was observed for the PFI-CNG system. Such an efficiency reduction can be explained mainly by the CNG combustion properties. The combustion of natural gas was slower and longer compared to gasoline fuel. The injected fuel mass was low at the 4.5 bar engine load point. The combustion duration became longer due to reduced engine speed, air motion in the cylinder and energy content. The CA10-90 engine map confirms that in the low load and low speed region, the combustion duration was longer by 2.5–3 CAD with the gaseous fuel (Fig. 5b and c).

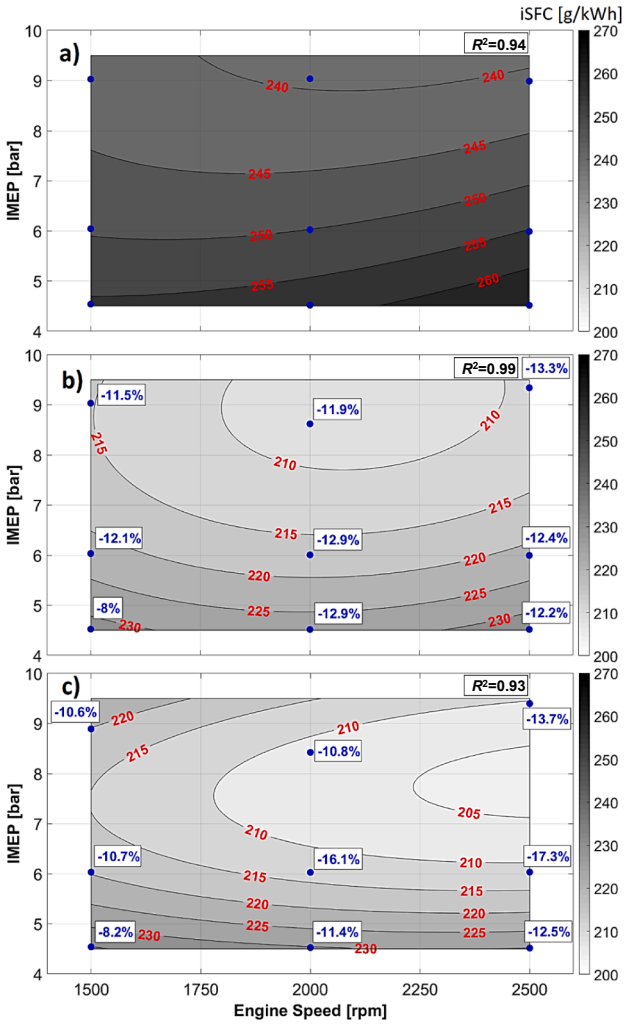

Fig. 7. iSFC (g/kWh) comparison between a) GDI, b) PFI-CNG and c) DI-CNG at different engine speeds and loads.

Fig. 7 presents iSFC surface maps for the GDI, PFI-CNG, DI-CNG injection systems.

iSFC values for GDI (Fig. 7a) were higher than those of PFI-CNG (Fig. 7b) and DI-CNG (Fig. 7c). The lower indicated specific fuel consumption for PFI-CNG and DI-CNG was mainly influenced by the higher LHV of natural gas of 47.27 MJ/kg vs. 42.79 MJ/kg for gasoline (~9.5% lower than CNG fuel). Thus, a lower injected fuel mass was required for the CNG cases. The biggest iSFC reduction with PFI-CNG was found at part/high load conditions. Considering that engines operate the majority of the time at part/high load at low/mid engine speeds in almost all driving cycles [38], the CNG fuel could give great benefits in CO_2 and fuel consumption reduction in different driving cycles (WLTC or RTS95). It is known that driving range for PFI-CNG vehicles can be an issue [48]. Additional benefits in driving range can be achieved with a DI-CNG system where the iSFC values were improved due to DI technology at part loads compared to PFI-CNG.

Comparing the measured and calculated parameters (p_{cyl}, RoHR, CoV_{IMEP}, CA10-90, iSFC), including the combined indirect measurement uncertainties, the CNG fuel clearly gave benefits of increased engine efficiency and lowered iSFC.

However, the combustion stability and duration suffered with gaseous fuels, especially with the PFI system. On the other hand, DI technology with gaseous fuels showed mainly benefits in all cases as the mentioned parameters were improved.

4.2. Engine standard emissions

The analysis of engine standard emissions is also presented as surface map plots showing the variation in standard emissions at different engine loads and engine speeds for the three different fuel injection systems. Standard emission measurements included indicated specific total hydrocarbons (iSHC), indicated specific carbon monoxide (iSCO), indicated specific carbon dioxide ($iSCO_2$) and indicated specific nitrous oxides ($iSNO_x$). Furthermore, an exhaust gas temperature map was included to support the exhaust gas emissions results.

Surface maps of iSHC are presented in Fig. 8. The iSHC values for GDI (Fig. 8a) decreased from ~6 g/kWh to 4.4 g/kWh with increasing engine load and speed. The highest iSHC emissions were observed in the low engine efficiency region, i.e., low load and engine speed of 1500–2000 rpm.

This can be attributed to combustion flame extinction in the bulk before the entire flame front reaches the cylinder wall [40]. Similar trends were observed by Sevik et al. [46]. Lower iSHC emissions at higher engine speed can also be influenced by better air and fuel mixing due to increased air motion. PFI-CNG (Fig. 8 b) tests showed that the iSHC emissions were ~2 times lower than for GDI under certain engine work conditions, i.e., 1500–2500 rpm low load or 2000–2500 rpm mid/high load map regions. The iSHC reduction was mainly attributed to the gas fuel composition, which had a lower proportion of carbon than gasoline. Like in the GDI tests, lower iSHC levels were obtained with PFI-CNG at higher engine speeds. Present study shows iSHC of total hydrocarbon emissions from CNG combustion. The emissions are not highlighted as methane or non-methane hydrocarbons. The major part (90–95%) of total hydrocarbon emissions from SI CNG engines is comprised of methane hydrocarbons [49]. Similar trends of high CH_4 emissions of THC were observed in duel fuel engine [50]. Even with the lean combustion or combustion improvement by H_2 addition the methane slip can not be avoided and CH_4 consisted a major part of the THC's [51].

iSHC emissions of the DI-CNG system (Fig. 8 c) showed very similar trends to those with PFI-CNG. iSHC varied from ~2.1 g/kWh at high speed/high load to ~2.5 g/kWh at mid/high load in the low speed region (Fig. 8c). DI-CNG iSHC exhaust gas emissions were improved at 1500 rpm and 9 bar IMEP compared to the PFI-CNG system. The PFI-CNG values were ~ 4.3 g/kWh, whereas DI-CNG achieved ~ 2.5 g/kWh. Hydrocarbon emissions were ~ 61% lower with DI-CNG compared

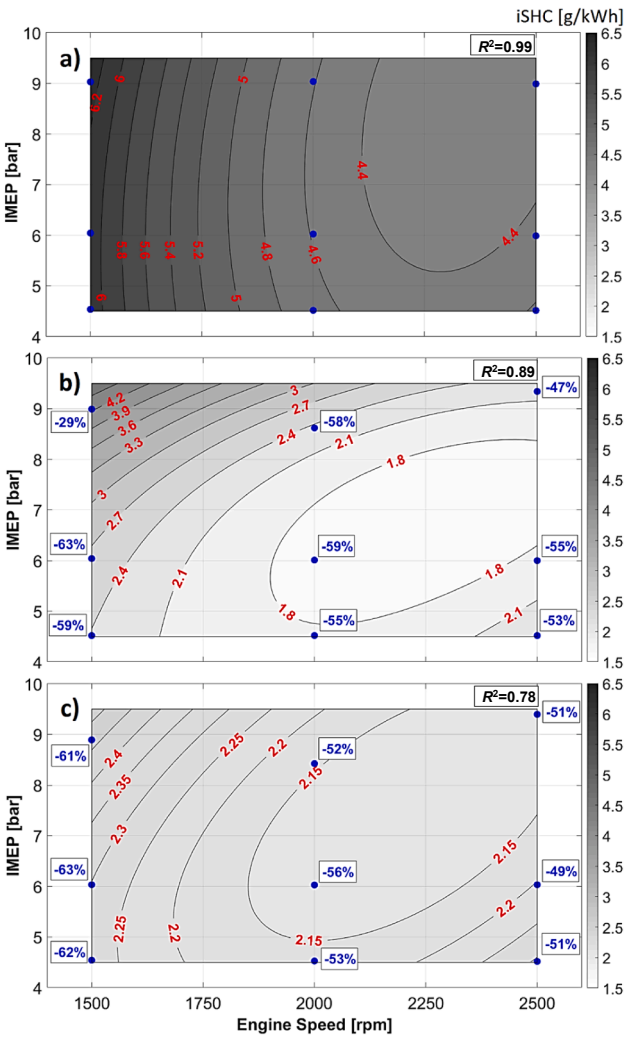

Fig. 8. iSHC (g/kWh) comparison between a) GDI, b) PFI-CNG and c) DI-CNG at different engine speeds and loads.

to GDI and ~ 45% lower compared to the PFI-CNG system. This reduction is very promising, even considering the calculated iSHC uncertainties (Table 6). The reduction of iSHC with the DI system was mainly influenced by an improved combustion process. The higher iSHC emissions for PFI-CNG are consistent with the results showing a shorter combustion duration for PFI-CNG (Fig. 5b) compared to DI-CNG (Fig. 5c). Thus, incomplete fuel combustion with the PFI system resulted in a shorter combustion duration and increased hydrocarbon emissions. However, the iSHC emissions were noticeably the highest for all three fuel injection systems in the high load (~9 bar IMEP) and low engine speed region at 1500 rpm compared to other engine working map areas. This trend of increased iSHC was likely due to flame quenching, where the combustion rate decreases as the temperature and pressure rapidly decrease. The iSHC emissions correlated with the combustion duration maps CA10-90 (Fig. 5). The combustion duration was the shortest at similar engine load and speed points. The increase of iSHC emissions for all injection systems at 1500 rpm engine speed may have been influenced by reduced air/fuel mixing in the cylinder due to less air motion.

The iSCO emissions maps for GDI, PFI-CNG and DI-CNG are presented in Fig. 9.

The GDI cases showed (Fig. 9 a) that carbon monoxide emissions gradually increased from ~ 17 to 18 g/kWh at low engine speed to ~ 24 g/kWh at higher engine speed. This was because the amount of injected fuel mass increased and the time to achieve complete combustion and

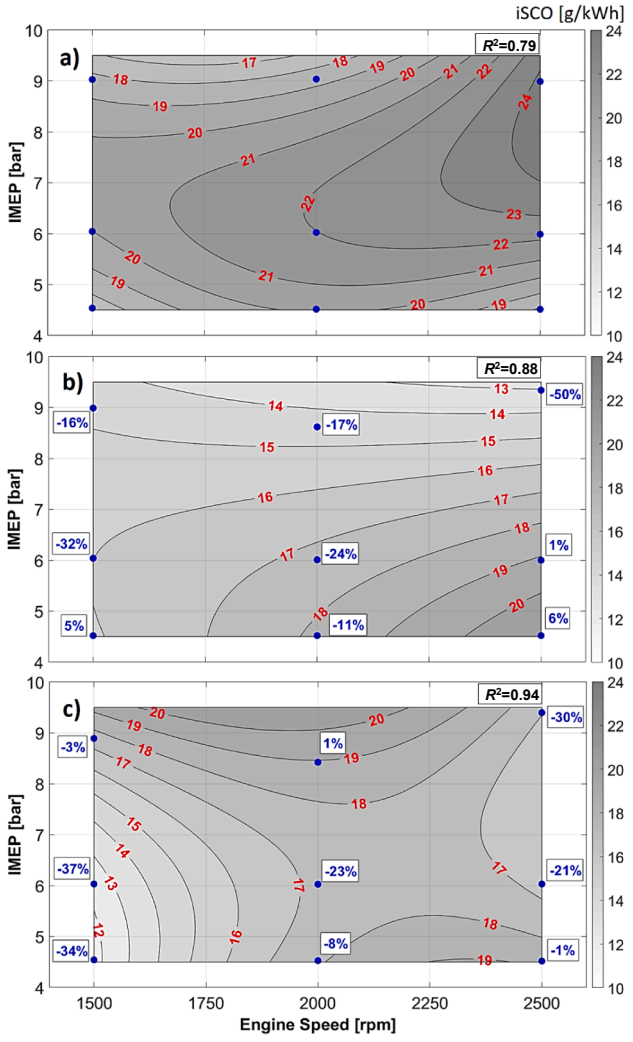

Fig. 9. iSCO (g/kWh) comparison between a) GDI, b) PFI-CNG and c) DI-CNG at different engine speeds and loads.

CO oxidation decreased with increasing engine speed.

A positive effect, i.e., reduction of iSCO emissions for CNG fuel, was observed in both the PFI and DI systems (Fig. 9b and c) at certain tested points. The decrease of iSCO was mainly attributable to the characteristics of methane, which has a higher H:C atom ratio (H:C = 3.72:1) compared to gasoline (H:C = 1.91:1). The lowest CO emissions for PFI-CNG were ~ 13–14 g/kWh at mid-speed (2000 rpm) and high speed (2500 rpm), high load points. In this map area, carbon monoxide emissions were decreased by around 50% with the CNG fuel compared with gasoline. However, the emissions increased at lower loads (4.5 bar IMEP) and especially at higher engine speed (2500 rpm) (iSCO = ~20 g/kWh). The main reasons for the increased CO emissions at the tested points were the lower injected fuel amount, reduced combustion temperature and shortened CO oxidation process time in the cylinder due to a higher engine speed. Kalam et al. also attributed an increase in CO to a lower combustion temperature [26].

A similar trend to that with PFI was observed with the DI-CNG system (Fig. 9c) in the low load and high engine speed area. The iSCO emissions were just slightly lower compared to the PFI-CNG and GDI cases. The iSCO map showed that the DI-CNG system provided benefits of CO reduction at low/mid load points in the 1500–2500 rpm engine speed range as DI promoted turbulence and an increased combustion temperature, enhancing the carbon monoxide oxidation process. The highest iSCO reduction (34–37%) compared to GDI was achieved with the DI-CNG system at low engine load and 1500 rpm. However, the DI-CNG tests showed that at high loads, CO emissions increased rapidly and exceeded those with PFI-CNG and GDI, especially at 1500–2000 rpm. This was attributed to worse air/fuel mixing and insufficient homogeneity in the cylinder. It is known that CO is formed by rich air/fuel mixtures when there is not enough oxygen present to fully burn all the carbon [26]. The combustion issues for DI-CNG were supported by iSHC data at the same tested points (1500–2000 rpm, 9–9.5 bar IMEP) (Fig. 8c) showing an increase compared to other DI-CNG engine speed and load points. This implied that the tested map area revealed issues associated with the combustion process.

Fig. 10 shows $iSCO_2$ emissions for the three fuel injection systems. The highest $iSCO_2$ emissions were observed at low load points and they decreased with increasing engine load from 4.5 bar to 9.5 bar IMEP.

The trends in CO_2 reduction were similar to those in the engine efficiency maps, i.e., at the most efficient engine points, the fuel iSFC and emitted CO_2 amount were the lowest. The tests showed that owing to its composition, use of the CNG fuel was able to reduce CO_2 emissions by up to 29% with the PFI system (Fig. 10b) compared with GDI.

An additional several percent reduction of CO_2 was achieved with the DI-CNG system (Fig. 10c), reaching up to ~ 32% lower CO_2 values compared to the gasoline cases. The highest benefit of the DI-CNG system was observed at high engine speed and mid/high engine load points, which correlated with the region of the engine maps where the efficiency was the highest (Fig. 6c) and iSFC the lowest (Fig. 7c).

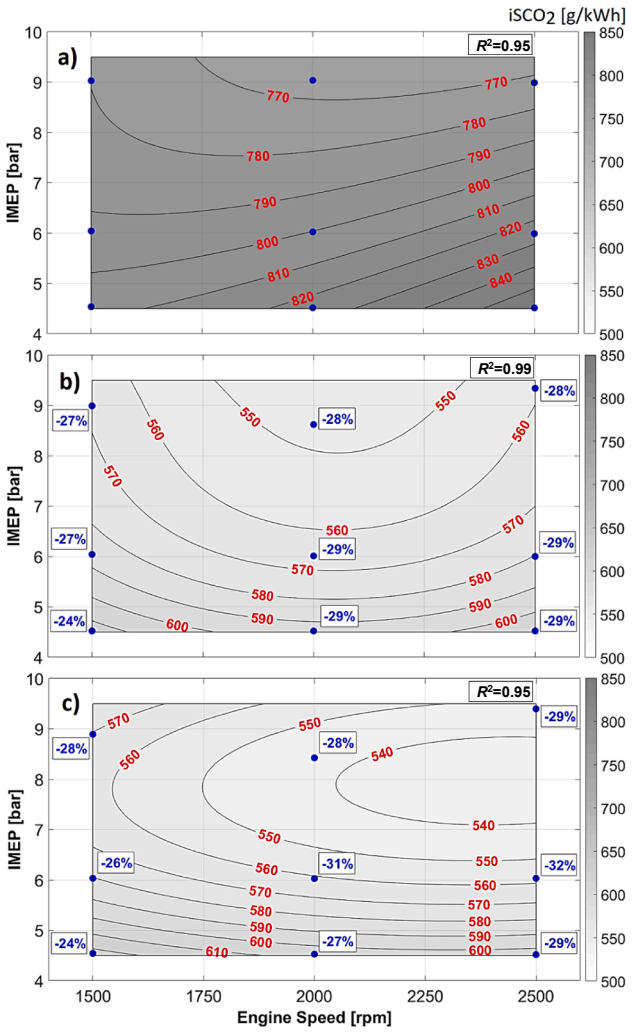

Fig. 10. $iSCO_2$ (g/kWh) comparison between a) GDI, b) PFI-CNG and c) DI-CNG at different engine speeds and loads.

Fig. 11 presents iSNO$_x$ emissions maps for the different fuel injection systems. As expected, the lowest iSNO$_x$ emissions were achieved for low load (4.5 bar IMEP) and low engine speed (1500 rpm).

Emissions increased with increasing engine speed and engine load with all three injection systems. The in-cylinder temperature increased with increasing engine load. Therefore, the NO$_x$ formation was higher. The increase in iSNO$_x$ for GDI (Fig. 11 a)) was from ~ 8 g/kWh at 4.5 bar IMEP and 1500–2000 rpm to 12.6–12.8 g/kWh at 9 bar IMEP 1500/2500 rpm. For PFI-CNG (Fig. 11b), the iSNO$_x$ increase was from 7.3 g/kWh to 12.8 g/kWh, and for DI-CNG case, the iSNO$_x$ increased from 7.1 g/kWh to 12.8 g/kWh at the same engine testing map points.

Comparison of the data for the three injection systems showed that iSNO$_x$ was reduced with the CNG fuel at part load points and mid and higher engine speeds. This reduction was attributed to the CNG fuel combustion characteristics, particularly a lower combustion temperature. In this area of the engine working map, DI-CNG showed the largest iSNO$_x$ decrease (9.5–15.3%) vs. GDI (Fig. 11c) and it was lower by several percent compared to PFI-CNG. However, the GDI tests showed that in the 4.5–6 bar IMEP and 1500 rpm engine speed region, iSNOx was even lower compared to some of the PFI-CNG and DI-CNG points. A slight increase of NO$_x$ emissions could be due to worse mixing of the gaseous fuel and air in the cylinder at low engine load and engine speed, which creates leaner air/fuel mixture areas. It is known that NO$_x$ formation is highly dependent on the combustion temperature. Under slightly leaner air/fuel mixture conditions, the combustion temperature increases, which in turn increases NO$_x$ formation. Similar iSNO$_x$ formation trends were reported by other research group [46], who showed that at some engine load points and low engine speeds, iSNO$_x$ with CNG fuel was slightly higher than with a GDI system and the greatest benefit was achieved with DI-CNG at part load conditions.

Fig. 12 shows the exhaust gas temperature for the GDI, PFI-CNG and DI-CNG systems.

The data support previously discussed results. The combustion process, RoHR and combustion temperature of natural gas were much lower than for the gasoline fuel. The combustion duration CA10-90 maps also indicated this, as discussed above (Fig. 5). A higher RoHR peak resulted in higher exhaust temperatures for the GDI case than for PFI-CNG and DI-CNG. However, the combustion was slightly improved with DI-CNG. In particular, the combustion duration was relatively shorter for DI-CNG, which means that the combustion was more intense and had a higher combustion temperature.

This resulted in a higher (by 5–16 °C) temperature (Fig. 12c) in the exhaust gases compared to the PFI-CNG system (Fig. 12b).

4.3. Engine exhaust particle measurements

4.3.1. Total PN measurements

Measurements of total PN for GDI, PFI-CNG and DI-CNG were also performed at various engine speeds and loads and are shown in the maps

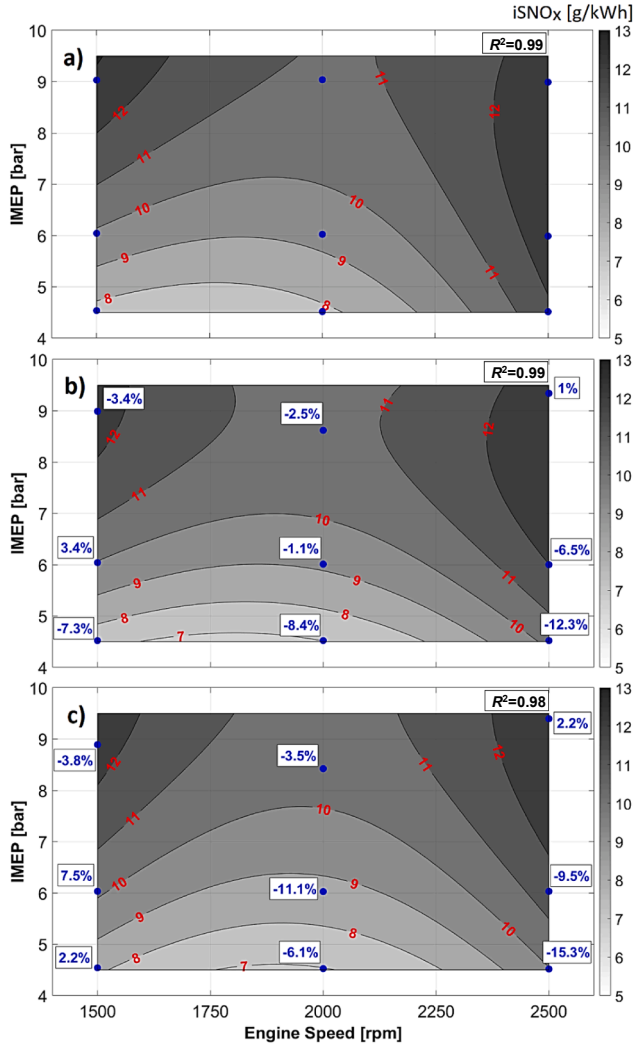

Fig. 11. iSNO$_x$ (g/kWh) comparison between a) GDI, b) PFI-CNG and c) DI-CNG at different engine speeds and loads.

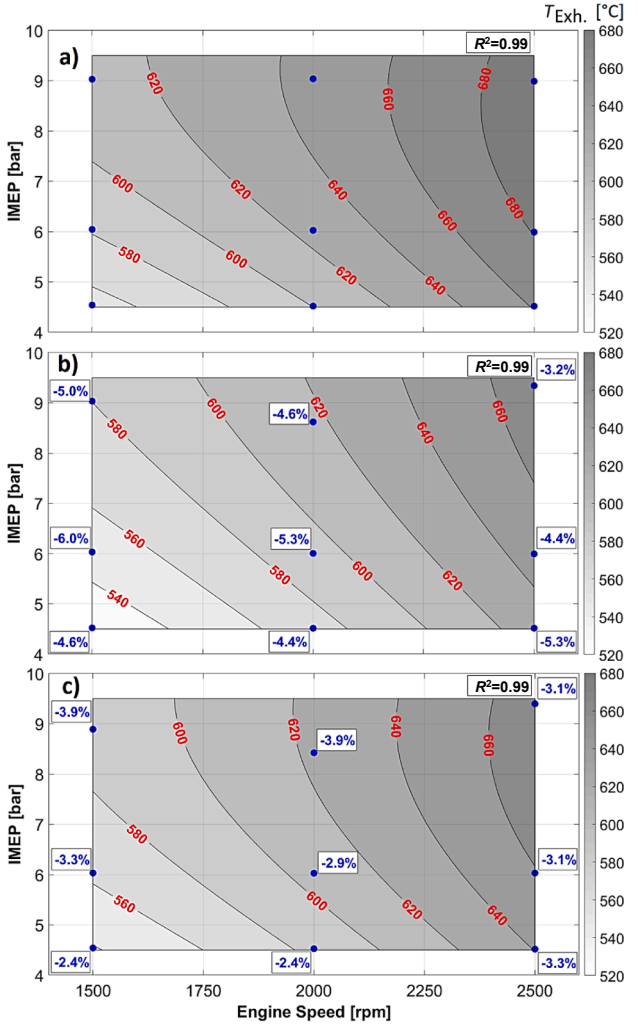

Fig. 12. Exhaust gas temperature (°C) comparison between a) GDI, b) PFI-CNG and c) DI-CNG at different engine speeds and loads.

in Fig. 13. The results showed that with increasing engine load, the total PN increased for all three combustion systems.

However, the maximum values for GDI (PN ~ 2.2 × 10^7) were one order of magnitude higher than for PFI-CNG (PN ~ 4.4 × 10^6) and DI-CNG (PN ~ 1.7 × 10^6). The highest PN value in the GDI case (Fig. 13a) was observed at 1500 rpm and 9 bar IMEP engine load, which was attributed to lower air/fuel mixing due to a less air motion at low engine speed and increased injected fuel mass needed for the high engine load. An increased engine speed promotes better air motion in the cylinder and achieves a more stoichiometric air/fuel mixture for the combustion. At high engine speeds, more aggressive air motion in the cylinder offsets the influence on air/fuel mixing time. Better mixture preparation and air motion improves the combustion efficiency, which promotes better soot oxidation and achieves higher levels of fully combusted products. Similar observations of decreased PN levels at higher engine speeds were mentioned by [52]. It was noted that at higher engine speeds the turbulence increased in the cylinder which enhanced the liquid fuel vaporization and improved air/fuel mixture. Increased piston wetting at low engine speeds compared to higher speeds was another reason of higher PN levels at 1500 rpm in a comparison with 2500 rpm in a present study. Increased piston wetting at low engine speeds was caused by an early injection timing (310 CAD bTDC) because the piston speed was low, and the piston was closer to TDC and GDI injector than at higher engine speed (2500 rpm). The total

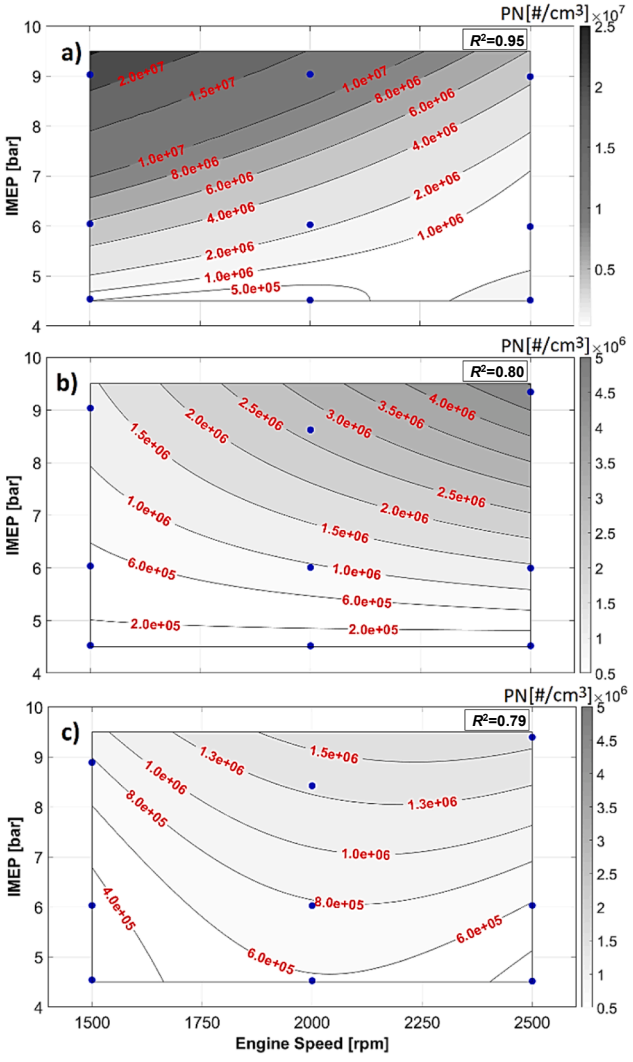

Fig. 13. Total PN comparison between a) GDI, b) PFI-CNG and c) DI-CNG at different engine speeds and loads.

PN decreased when the piston positioning was lower in the cylinder at higher engine speed. Piston wetting is one of the main particles generating paths in GDI engines [52]. It was stated that engine soot out emissions are influenced by a fuel film distribution, mass and thickness [53]. One of the solutions is to retard the injection timing, however, it can cause other issues related with insufficient time for mixture formation, rich mixture formations at the cylinder crevices which can also increase the THC emissions [54].

Tests with the CNG fuel revealed that the total PN was lower with PFI and DI compared to the gasoline tests. The reduction of particulates from natural gas was mainly attributed to the fuel characteristics. The methane-based fuel had a higher H:C ratio than gasoline, which meant that less carbon was involved in the combustion and fewer carbon-based particulates were produced.

The trends in PN formation with engine speed were different for the PFI-CNG (Fig. 13b) and GDI cases. For PFI-CNG, the highest PN was measured at the highest engine speed (2500 rpm) and engine load (9 bar IMEP), whereas the lowest PN (PN ~ 1.5 × 10^5) was achieved at the lowest engine speed (1500 rpm) and low load point (4.5 bar IMEP). The trend of increasing PN related with engine load was similar for both GDI and PFI-CNG systems. Either in GDI, either in PFI-CNG cases the PN increased when the load was increased. A higher engine load requires more fuel to be injected, and a larger amount of air/fuel mixture produces a larger PN in the exhaust. With increasing engine speed, higher PN numbers are obtained due to the shorter time for mixing and combustion. It is known that CNG fuel can have issues in mixing with air in the intake manifold. PFI-CNG parameters, such as the distance of the injector from the intake valves and positioning angle can have an influence on the engine combustion process, engine efficiency and emissions formation [55]. Herrera et al. [56] have advised that a PFI-CNG system should be optimized with respect to location, position, angle and geometry of the nozzle in order to achieve a proper combustible mixture. In the present study, we showed that the methane-based fuel also had a longer combustion process, which possibly contributed to the higher PN observed at higher engine speeds.

The DI-CNG tests (Fig. 13c) revealed that PN was reduced compared to the PFI-CNG and especially GDI systems. Values of PN with DI-CNG were around 3 times lower than those with PFI-CNG in the 2500 rpm and 9 bar IMEP map region. In other engine working map areas, the total PN was slightly lower with GDI than with PFI. However, the correlation between engine load and speed was the same as for the PFI-CNG system. The PN reduction with DI-CNG compared to PFI could be caused by several phenomena. Firstly, iSFC was lower with DI-CNG than with PFI-CNG. It is known that soot formation depends on the injected fuel mass. Thus, lower fuel consumption in the DI-CNG system could have led to lower PN formation. Secondly, analysis of the combustion duration CA10-90 showed that DI-CNG had slightly shorter combustion due to a higher rate of heat release. It was mentioned before that use of a DI-CNG system increases the flame propagation speed due to increased air/fuel mixture motion and turbulence in the cylinder. The increased flame propagation speed enables higher combustion temperatures to be achieved because of higher RoHR (Fig. 3) and better soot oxidation at later combustion phases.

Additional comparison of iSHC emissions and different PN size ranges (10–23 nm and 23–1000 nm) between GDI, PFI-CNG and DI-CNG is presented in Fig. 14. The comparison aims to show possible correlations between hydrocarbons and engine soot out emissions. It is known that nucleation mode particles are more volatile organic compounds (VOCs) with a footprint from the fuel and oil [57]. VOCs are defined as organic compounds and include more than 300 different chemical structures, such as aldehydes, ketones, alkanes, aromatic hydrocarbons, alkenes and halogenated hydrocarbons. It has been reported that VOCs are mainly unburnt or partially burnt fuel or are formed from the evaporation of different fuel additives and lubricants [58]. VOCs should be avoided as they generally have high toxicity, which can damage human health and the environment. Previous GDI tests with a

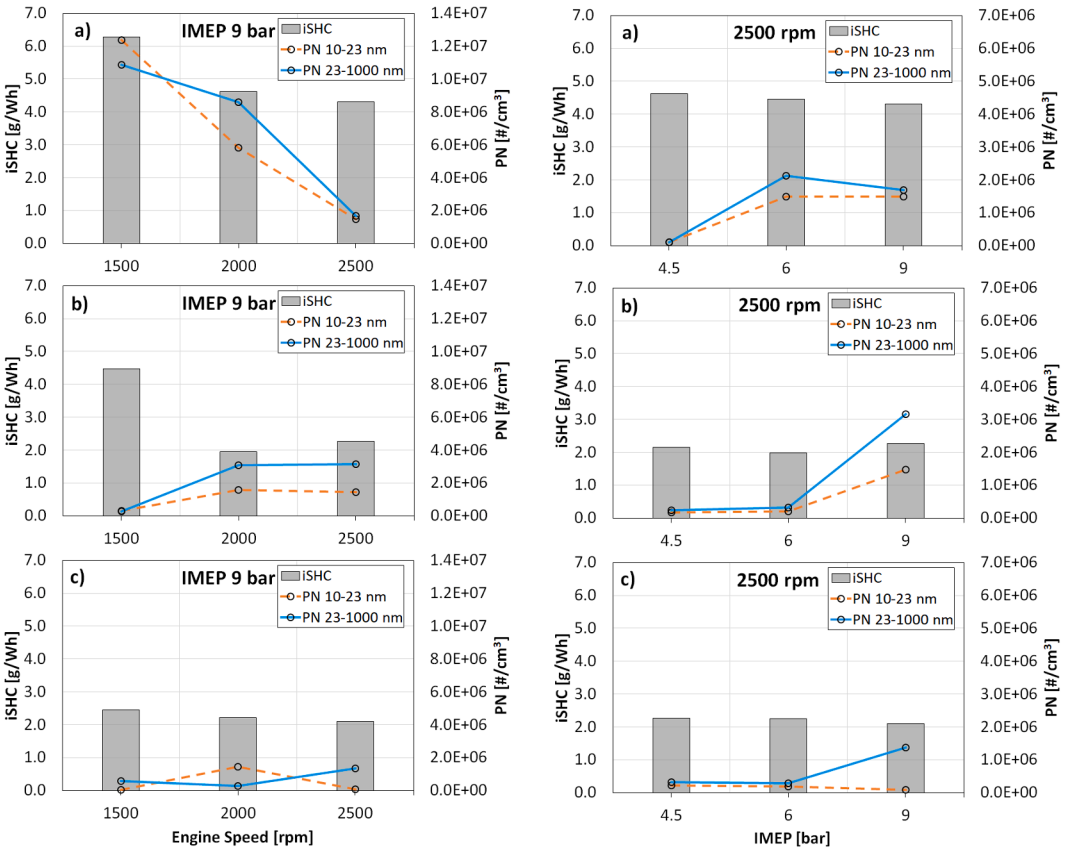

Fig. 14. Comparison of iSHC and PN size ranges for a) GDI, b) PFI-CNG and c) DI-CNG. Left column -fixed load, varying speed; right column – fixed speed, varying load.

thermodenuder showed that the majority of VOCs can be removed from raw emissions [59].

Fig. 13 showed that PN formation for GDI cases was more influenced by the engine speed while the PN emissions for PFI-CNG and DI-CNG were dominated by the engine load. Fig. 14 (left column) shows that iSHC together with PN emissions (at different particle size ranges) decreased when the engine speed was increased from 1500 rpm to 2500 rpm (at the same engine load ~ 9 bar IMEP). As it was mentioned before, the main cause of increased iSHC and PN emissions at lower engine speed was piston wetting and increased amount of unburnt fuel. The analysis shows that PN in a size range of 10–23 nm at 1500 rpm was also higher compared to accumulation mode particles (23–1000 nm) which proves that hydrocarbons play one of the main roles in volatiles and smaller particle size formation. The iSHC and PN emissions correlates with a decreasing trend when the engine speed increases. Piston positioning in the cylinder is lower from the GDI injector at 2500 rpm which gives less liquid spray on the piston surface and less iSHC and PN emissions. Opposite trend was observed with PFI-CNG and DI-CNG systems when engine speed increased. Increased engine speed improved the iSHC emissions slightly, however, the PN trend was different from the GDI case.

Fig. 14 (right column) shows the comparison of different injection systems at constant engine speed (2500 rpm) but at different engine loads (4.5, 6, 9 bar IMEP). PN emissions from PFI-CNG and DI-CNG systems were more influenced by the engine load change, but the changes in iSHC were minor and very similar between different gaseous systems. The biggest number of PN for PFI and DI-CNG were emitted in the size range of 23–1000 nm. However, DI-CNG system showed that it can emit the lowest PN emissions at different PN size ranges compared with two other fuel injection systems.

Summarizing the analysis results of total PN, the combination of natural gas and a DI system could aid PN reduction at stoichiometric conditions. This combination was found to be beneficial compared to PFI-CNG and especially GDI combustion.

4.3.2. *Particle size distribution maps*

Figs. 15–17 show particle size distribution maps for the different fuel injection systems based on engine speed at different engine loads. The plots represent the number concentration of particles per unit flow ($dN/dLogDp/cm^3$) as a function of particle size, which varied from 7 nm to 300 nm diameter. The measurements revealed the same correlation between engine load and particle number concentration (PNC). PNC increased due to the larger amount of injected fuel required to achieve higher loads. However, the trends in particle size distribution differed among the fuel injection systems.

Analysis of the GDI (Fig. 15) test results showed that the particulate concentration was the highest ($\sim 3.0 \times 10^6$ #/cm^3) for ~12 nm particle size, the lowest engine speed (1500 rpm) and highest engine load (9 bar IMEP). Higher peaks at low engine speed can be explained by worse air/fuel mixing and issues in achieving proper stoichiometric conditions, as discussed before. The air motion is not sufficiently turbulent to be properly mixed with a large amount of injected fuel at low engine speeds. Therefore, rich regions of air/fuel mixture appear. This explanation can again be supported by the iSHC map (Fig. 8a), which showed that in the same engine working map area, emissions of THC were slightly higher, indicating that the flame was quenched and the combustion rate decreased, resulting in a rapid temperature and pressure decrease in the cylinder. As it was mentioned before, higher hydrocarbon formation can lead to an increased particle concentration in the nucleation mode (10–20 nm). Another peak was observed at 70–100 nm when testing at a high engine load with the GDI system. This peak was attributed to particles in the accumulation mode and reached ~8.0 ×

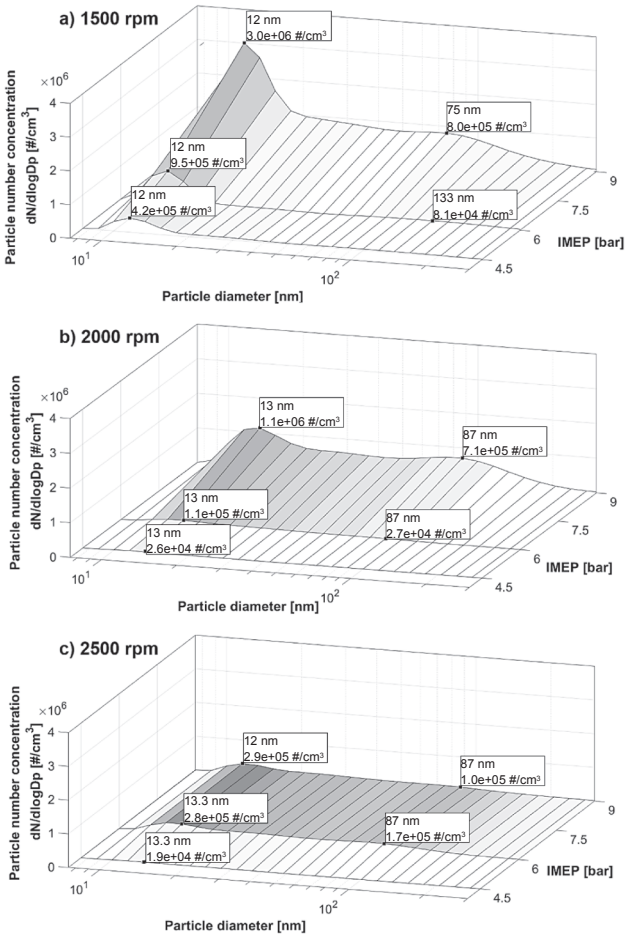

Fig. 15. Dependence of particle size distribution on engine load and engine speed for the GDI system.

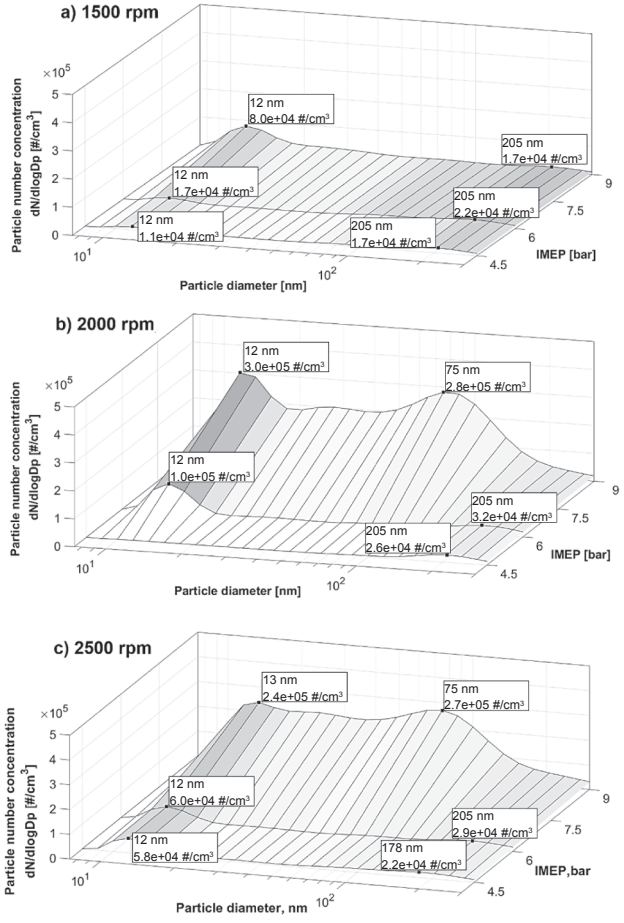

Fig. 16. Dependence of particle size distribution on different engine loads and engine speeds for the PFI-CNG system.

10^5 #/cm^3 at the lowest engine speed (1500 rpm). It has been suggested that accumulation mode particles are formed when fuel molecules undergo pyrolysis at high temperatures, where primary particles (5–30 nm) grow into spheres [57]. When the temperature decreases, nucleation particles participate in the coagulation process where coalescence occurs. This means that two particles collide in a reactive manner and form a new, broadly spherical particle [57].

The total PN was found to decrease when the engine speed was increased up to 2500 rpm in the GDI system (Fig. 15c). This can also be seen from the particle size distribution as the highest peaks corresponding to the nucleation and accumulation modes decreased at all load points (Fig. 15). Although the mass flow rate was higher at higher engine speeds, the formation of both small and large sized particles was lower. Lower PN formation was likely influenced by better combustion and fuel oxidation processes at higher engine speeds due to enhanced air motion and mixing of air with the fuel in the cylinder. It is known that oxidation reduces the mass of polycyclic aromatic hydrocarbons (PAHs), which is a cause to form soot particles and soot precursors. Increased oxidation helps to avoid soot formation and increase CO and CO_2 formation [57].

The particle size distribution for the PFI-CNG system is presented in Fig. 16. The PFI-CNG tests showed that the PN values for the nucleation and accumulation modes were mostly one order of magnitude lower than for the GDI cases. Lower soot formation for the natural gas fuel was likely influenced by the fuel composition as it had a higher H:C ratio than the gasoline fuel. Natural gas is a methane-based fuel which has the lowest molecular weight among hydrocarbons. Also, it does not have carbon to carbon molecular bonds and has a simpler molecular structure than gasoline fuel. A lack of carbon to carbon bonds leads to a substantially lower probability of benzene ring formation and lower soot formation [30].

The trend of increasing PNC for particles of certain sizes as the engine load was increased was similar for PFI-CNG, and GDI. A higher engine load requires more fuel, increasing the amount of soot formation.

However, the particle size distribution plots showed that the number of nucleation and accumulation mode particles increased with increasing engine speed from 1500 to 2500 rpm.

The highest PNC was at 13 nm (nucleation mode particles), especially at the highest engine load points (~9 bar IMEP) and engine speeds (2000–2500 rpm). A similar trend of the highest peaks for 10 nm particle size was observed by Thiruvengadam et al. when a PFI-CNG system (HD engine) was tested at cruise driving conditions [31]. In the present study, accumulation mode peaks were observed at 75–200 nm, especially at 6–9 bar IMEP and engine speeds above 1500 rpm. A lower number of accumulation mode particles (100–300 nm) was also determined by other scientists when CNG was tested with a PFI system [60].

The lower levels of soot formation at low engine speed and low-mid engine load using PFI-CNG were likely influenced by the oxidation time. A low engine speed is able to ensure a longer time for oxidation, reducing soot production. The iSCO (Fig. 9b) and iSCO$_2$ (Fig. 10b) results also demonstrated that more CO and CO_2 standard emissions were generated instead of soot due to a longer oxidation process at 1500 rpm. Other researchers have also noted that with lower engine speeds, more available time is available for oxidation during the expansion stroke. Conversely, an increased engine speed resulted in an increase of emitted particles [61].

Tests with the PFI-CNG system at low engine speed (1500 rpm) revealed that nucleation mode particles reached 1.5×10^4–8.0×10^4

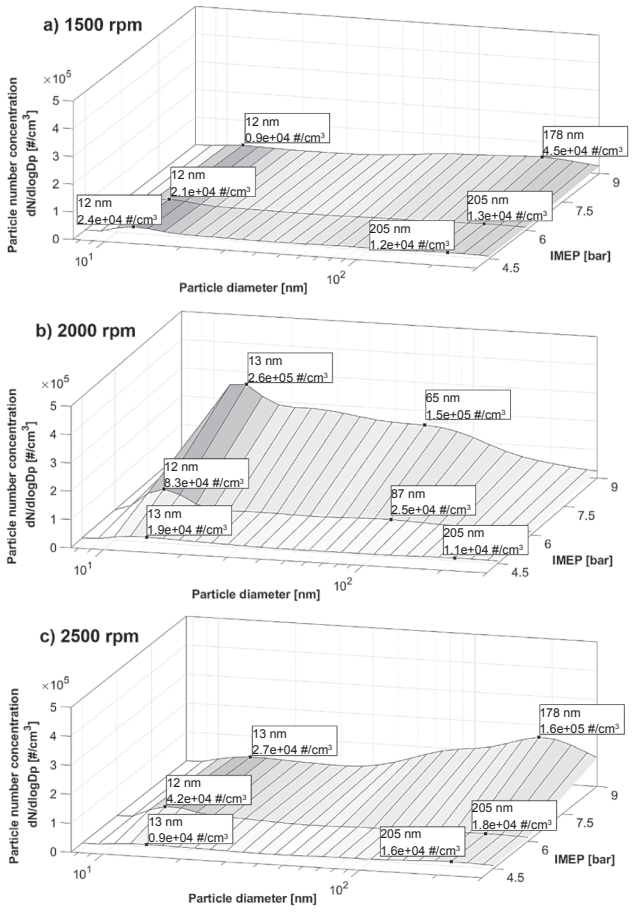

Fig. 17. Dependence of particle size distribution on different engine loads and engine speeds for the DI-CNG system.

#/cm^3 PNC depending on the engine load. At the highest engine speed (2500 rpm), the nucleation mode PNC reached up to 5.8×10^4–2.4×10^5 #/cm^3. Thus, it was one order of magnitude higher at 9 bar IMEP and 2500 rpm compared to 1500 rpm. As mentioned above, nucleation particles contain more VOCs with a footprint from the fuel and oil. Another study has shown that 77% of nucleation mode particles (<25 nm) emitted from a CNG HD engine were volatile based compounds [62]. It is likely that nucleation mode particles in the present study were mainly composed of VOCs originating from the oil as methane-based fuels have a tendency to soot less because of the fuel's composition. Other studies have shown that a CNG SI engine (HD engine with PFI system) generates nucleation mode particles originating from the lubrication oil [29,30]. It has been suggested that the main soot emission source is partial combustion from lubrication oil because of piston ring dynamics [60]. Also, engine wear metals have been found to make up a fraction of PM [30]. The largest amounts detected in PM emissions were Ca, Mg, Zn, S, P elements usually present in lubrication oil as additives, whereas elemental carbon and organic carbon were a minor part in the PM elemental fraction analysis [31]. Although PNC was higher for smaller particles than larger ones, it was claimed that smaller particles did not make a significant contribution to PM mass emissions. Therefore, the particulate mass was mainly attributed to accumulation mode particles [31,60].

Several reports have mentioned that the main soot production source when CNG is used as a fuel is combustion of an oil film on the cylinder walls. However, soot formation due to the CNG fuel should not be ruled out because interesting nucleation and accumulation mode particle formation trends were observed in the present study at high engine speeds (2000–2500 rpm) and engine loads (9 bar IMEP). The PFI-CNG tests showed that stronger accumulation mode particle peaks appeared at the highest engine load (9 bar IMEP) and speed (2000–2500 rpm). The concentration of 75 nm particles (2.8×10^4 #/cm^3) was almost the same as that of nucleation mode particles (3.0×10^5 #/cm^3) at 2000 rpm. At the highest engine speed (2500 rpm), the concentration of accumulation mode particles at 75 nm was slightly higher than 13 nm nucleation mode particles. Such increases in nucleation and accumulation mode particles and changes in the peaks are likely related to PAH formation and particle coagulation and agglomeration, which depend on various thermal and turbulent processes. Previous fundamental studies of methane flame combustion have shown that increasing the amount of methane together with a constant carbon content increased the concentrations of PAHs and soot. It has been reported that methane has a synergy with other alkanes to produce PAHs due to its ability to produce methyl radicals [63]. Other studies, in which a CNG bus vehicle was tested at different driving cycles, showed that various emissions of VOCs, particle associated PAHs and semi-volatile PAHs were detected, with especially higher levels for more intense driving cycles [64]. It is known that PAHs are generated from hydrogen, hydroxide OH, methyl CH_3 radical molecules and organic compounds, such ethylene C_2H_4 and acetylene C_2H_2, during thermal pyrolysis [57,65]. New particles are created during this polymerization with sizes of 5–30 nm. After the temperature starts to decline, nucleation particles coagulate into groups of particles of 70–100 nm. Later, these particles collide with each other in the exhaust-system branch and agglomerate. The agglomeration can be influenced by thermal or turbulent processes [65]. In the present study, the high engine load tests at higher engine speeds (Fig. 16b and c) required a higher fuel amount to be injected. Therefore, a larger amount of PAHs was likely formed and involved as precursors of soot formation. As the combustion temperatures decreased, part of the nucleation particles coagulated and agglomerated, which gave an accumulation mode peak at 75 nm (Fig. 16b). As mentioned before, the highest engine speed (2500 rpm) (Fig. 16c) showed a slightly higher accumulation mode peak compared to 2000 rpm. This increase may have been influenced by the larger amount of combusted fuel, increased turbulence in the cylinder and shorter combustion duration (Fig. 5b)) at the higher engine speed.

PNC measurements of DI-CNG (Fig. 17) showed that the concentrations were at similar levels to those with PFI-CNG and mainly lower by one order of magnitude compared to the GDI cases.

The PNC per volume increased with increasing engine load because the injected fuel amount was larger at higher engine load. Similar trends in the nucleation and accumulation mode particle peaks were observed with the DI-CNG system as for PFI-CNG. Higher engine speeds (2000–2500 rpm) with DI-CNG resulted in higher PNCs being emitted at high engine load points (9 bar IMEP) compared to at 1500 rpm. However, the PNC values for the nucleation or accumulation mode were still lower than for GDI by one order of magnitude at certain load points. Comparison between the results for PFI-CNG and DI-CNG revealed that the trends in nucleation and accumulation mode particle formation were similar between the injection systems depending on the engine load and engine speed.

The highest PNC ($\sim 2.6 \times 10^5$ #/cm^3) of the nucleation mode at 13 nm was detected for DI-CNG in the region of 9 bar IMEP load and 2000 rpm engine speed (Fig. 17b), with some rise in the accumulation mode region. Measurements at higher engine speeds (2500 rpm) (Fig. 17c) with DI-CNG showed that the levels of nucleation and accumulation mode particles were slightly decreased compared to at 2000 rpm. Similar trends in PNC for different diameter particles were observed with DI-CNG as with PFI-CNG at the same engine load point (9 bar IMEP) and engine speeds (2000 and 2500 rpm). The accumulation mode (at 178 nm) particle concentration was higher than the nucleation mode (at 13 nm) particle concentration at 2500 rpm, but the opposite trend was detected at 2000 rpm. This finding agrees with the PFI-CNG results, which showed that changes in the highest peaks at different engine speeds were likely due to changed turbulence conditions in the cylinder, which in turn influenced the combustion and particle type formation. Changing particle formation trends at different engine speeds with gaseous fuel were also observed by Amirante et al. [61]. Tests at

different engine speeds of 2000, 3000 and 4000 rpm showed different effects on the PN, particularly at 3000 rpm. This was explained as changes in the turbulence conditions, demonstrating that soot formation is sensitive to the thermo-physical combustion conditions [61].

Another advantage of DI-CNG should be highlighted, i.e., the PNC peaks of small and large diameter particles were lower at the mid load point (6 bar IMEP) and 2000–2500 rpm engine speed with DI-CNG than with PFI-CNG. The lower PN formation with DI-CNG was attributed to lower fuel consumption (Fig. 7b) and c) at the same tested points and correlated with the total PN data (Fig. 13c) showing that the total PN values for DI-CNG were lower than for PFI-CNG.

Summarizing the PN formation tendencies with the different fuel injection systems, it can be concluded that the CNG fuel emitted lower engine soot emissions in most of the tested engine regimes compared with the gasoline fuel. An additional advantage of the DI-CNG system was the total PN levels were lower than for PFI-CNG. Another benefit of the DI-CNG system is the gaseous fuel can be injected early during the intake stroke without wetting the piston, in contrast to GDI combustion.

5. Conclusions

Spark ignition engine tests with different fuel injection systems suggested the following main conclusions:

1. The RoHR and CA10-90 analysis showed that the highest combustion heat release rate was achieved with the GDI system, whereas RoHR of the CNG fuel was slightly lower with the PFI and DI systems. CA10-90 was longer by 0.5 to 3 CAD with PFI-CNG and DI-CNG compared to GDI depending on the engine speed and load. Longer combustion with the CNG fuel was mainly due to worse natural gas combustion properties. However, a comprehensive combustion analysis showed that the DI system with gaseous fuel provided an additional benefit of increased turbulence in the cylinder, which increased the combustion rate and had an influence on the exhaust gas emissions.
2. Although CNG showed worse combustion properties compared to gasoline, CoV_{IMEP} was sufficiently low (below 1.5%) with the DI-CNG system to achieve a similar combustion stability level as with GDI at various engine speeds and loads. In contrast, the combustion stability with PFI-CNG was highly dependent on the engine load and CoV_{IMEP} varied from 0.9% to 3%.
3. The CNG fuel achieved a higher engine efficiency and lower indicated specific fuel consumption with the PFI and DI systems at most tested engine points due to the higher energy content of natural gas. The highest (8% to 10%) improvement in the engine efficiency compared to GDI was achieved with DI-CNG at 6 bar IMEP load and 2000–2500 rpm engine speed. This was due to an enhanced combustion process by the directly injected gas and higher turbulence in the cylinder.
4. CNG application had a significant effect in reducing standard emissions compared to the gasoline fuel. In certain engine working map areas, iSHC, iSCO, $iSCO_2$ and $iSNO_x$ were reduced by 63%, 37%, 32% and 15.3%, respectively, with natural gas fuel compared to the equivalent values with gasoline. DI-CNG had the highest impact on standard exhaust gas emissions reduction at low and part load conditions.
5. Use of a high engine load at low engine speed led to increased total particle number formation with the GDI system. The increase was attributed to reduced air/fuel mixing due to less air motion in the cylinder and an early injection timing, which created a soot source because of piston wetting. For PFI-CNG and DI-CNG, the particle number was lower in all tested engine regimes compared to gasoline, mainly due to the lower carbon amount in the gaseous fuel.
6. Soot formation with the CNG fuel was mainly influenced by the available time for air/fuel mixing and combustion. PN increased at higher engine speeds with both PFI-CNG and DI-CNG, but it was still lower than with GDI. DI-CNG showed additional advantages over PFI because it could achieve an increased rate of combustion, RoHR and lower fuel consumption, resulting in lower particle number formation.

CRediT authorship contribution statement

Mindaugas Melaika: Conceptualization, Methodology, Software, Formal analysis, Investigation, Resources, Data curation, Writing - original draft, Writing - review & editing, Visualization. **Gilles Herbillon:** Conceptualization, Methodology, Resources, Data curation, Writing - original draft. **Petter Dahlander:** Conceptualization, Methodology, Software, Formal analysis, Investigation, Resources, Data curation, Writing - original draft, Supervision, Project administration, Funding acquisition.

Declaration of Competing Interest

The authors declare that they have no known competing financial interests or personal relationships that could have appeared to influence the work reported in this paper.

Acknowledgements

We gratefully acknowledge the financial support from the Swedish Energy Agency (Project number P44829-1). Also, authors like to acknowledge the GDTech company for valuable inputs about the DI-CNG injection system.

References

[1] European Commission, Reducing CO2 Emissions from Passenger Cars, Available from European Commission from https://ec.europa.eu/, July 2012.
[2] European Council, CO2 emission standards for cars and vans. Accessed on 2020 April. Available on: https://www.consilium.europa.eu/en/press/press-releases/2019/01/16/co2-emission-standards-for-cars-and-vans-council-confirms-agreement-on-stricter-limits/.
[3] United States Environmental Protection Agency, Final Rule for Model Year 2017 and Later Light-Duty Vehicle Greenhouse Gas Emissions and Corporate Average Fuel Economy Standards. Accessed on 2020 April. Available on: https://www.epa.gov.
[4] DieselNet Engine & emission technology online. Accessed on 2020 April. Available on: https://dieselnet.com/standards/eu/ld.php.
[5] The International Council on Clean Transportation ICCT. CO2 Standards for Heavy Duty Vehicles in the European Union. Accessed on 2020 April. Available on: https://theicct.org/sites/default/files/publications/CO2%20HDV%20EU%20Policy%20Update%202019_04_17.pdf.
[6] European Commission. Sustainable Transport. Accessed on 2020 April. Available on: https://ec.europa.eu/transport/themes/sustainable_en.
[7] European Commission. Electrification of the Transport System. Studies and Reports. Accessed on 2020 April. Available on: https://ec.europa.eu/programmes/horizon2020/en/news/electrification-transport-system-expert-group-report-0.
[8] Suarez-Bertoa R, Astorga C. Unregulated emissions from light-duty hybrid electric vehicles. Atmos Environ 2016;136:134–43. https://doi.org/10.1016/j.atmosenv.2016.04.021.
[9] Zirn O, Krauth S, Ahlborn M. Hybridisation potentials for heavy trucks considering route topography. IFAC-PapersOnLine 2016;49–21:316–21. https://doi.org/10.1016/j.ifacol.2016.10.575.
[10] Rousseau, A., "Fuel Efficiency Benefits of Electrified CNG Vehicles," 2013 World Electric Vehicle Symposium and Exhibition (EVS27): 1-8, 2013, doi:10.1109/EVS.2013.6915030.
[11] Arat HT. Alternative fuelled hybrid electric vehicle (AF-HEV) with hydrogen enriched internal combustion engine. Int J Hydrogen Energy 2019;44:19005–16. https://doi.org/10.1016/j.ijhydene.2018.12.219.
[12] Melaika, M., Mamikoglu, S., and Dahlander, P., "48V Mild-Hybrid Architecture Types, Fuels and Power Levels Needed to Achieve 75g CO2/km," SAE Technical Paper 2019-01-0366, 2019, doi: 10.4271/2019-01-0366.
[13] Song H, Liu C, Li F, Wang Z, He X, Shuai S, et al. A comparative study of using diesel and PODEn as pilot fuels for natural gas dual-fuel combustion. Fuel 2017;188:418–26.
[14] You J, Liu Z, Wang Z, Wang D, Xu Y, Du G, et al. The exhausted gas recirculation improved brake thermal efficiency and combustion characteristics under different intake throttling condition of a diesel/natural gas dual fuel engine at low loads. Fuel 2020;266:117035. https://doi.org/10.1016/j.fuel.2020.117035.
[15] Yazdanie M, Noembrini F, Dossetto L, Boulouchos K. A comparative analysis of well-to-wheel primary energy demand and greenhouse gas emissions for the

operation of alternative and conventional vehicles in Switzerland, considering various energy carrier production pathways. J Power Sour 2014;249:333–48. https://doi.org/10.1016/j.jpowsour.2013.10.043.
[16] Angelidaki I, Treu L, Tsapekos P, Luo G, et al. Biogas upgrading and utilization: Current status and perspectives. Biotechnol Adv 2018;36:452–66. https://doi.org/10.1016/j.biotechadv.2018.01.011.
[17] Bhasker JP, Porpatham E. Effects of compression ratio and hydrogen addition on lean combustion characteristics and emission formation in a Compressed Natural Gas fuelled spark ignition engine. Fuel 2017;208:260–70. https://doi.org/10.1016/j.fuel.2017.07.024.
[18] Hora TS, Agarwal AK. Experimental study of the composition of hydrogen enriched compressed natural gas on engine performance, combustion and emission characteristics. Fuel 2015;160:470–8. https://doi.org/10.1016/j.fuel.2015.07.078.
[19] Duc KN, Duy VN, Hoang-Dinh L, Viet TN, Le-Anh T. Performance and emission characteristics of a port fuel injected, spark ignition engine fueled by compressed natural gas. Suistain Energy Tecnol Assessm 2019;31:383–9. https://doi.org/10.1016/j.seta.2018.12.018.
[20] Hall, J., Hibberd, B., Streng, S. and Bassett, M., "Compressed-natural-gas optimized downsized demonstrator engine," Proc IMechE Part D: J Automobile Engineering 232(1):75–89, 2018, doi:10.1177/0954407017707552.
[21] Isenstadt A., German J., Dorobantu M., Boggs D., Watson T. Downsized, boosted gasoline engines. The International Council on Clean Transportation. Working paper 2016-21. October 2016: 23 p. https://theicct.org/publications/downsized-boosted-gasoline-engines.
[22] Hofmann P, Hofherr T, Hoffmann G, Preuhs JF. Potential of CNG direct injection for downsizing engines. MTZ Worldwide 2016;77(7–8):28–35. https://doi.org/10.1007/s38313-016-0074-6.
[23] Moon S. Potential of direct-injection for the improvement of homogeneous-charge combustion in spark-ignition natural gas engines. Appl Therm Eng 2018;136:41–8. https://doi.org/10.1016/j.applthermaleng.2018.01.068.
[24] Sankesh D, Edsell J, Mazlan S, Lappas P. Comparative study between early and late injection in a natural-gas fuelled spark-ignited direct-injection engine. Energy Procedia 2017;110:275–80.
[25] Chen L, Wei H, Zhang R, Pan J, Zhou L, Liu C. Effects of late injection on lean combustion characteristics of methane in a high compression ratio optical engine. Fuel 2019;255:115718. https://doi.org/10.1016/j.fuel.2019.115718.
[26] Kalam M.A., Masjuki H.H. An experimental investigation of high performance natural gas engine with direct injection. Department of Mechanical Engineering, University of Malaya, 50603 Kuala Lumpur, Malaysia. Energy 36 (2011) 3563-3571.
[27] Baratta M, Rapetto Nicola. Mixture formation analysis in a direct-injection NG SI engine under different injection timings. Fuel 2015;159:675–88. https://doi.org/10.1016/j.fuel.2015.07.027.
[28] McTaggart Cowan GP, Rogak SN, Munshi SR, Hill PG, Bushe WK. The influence of fuel composition on a heavy-duty, natural-gas direct-injection engine. Fuel 2010;89:752–9. https://doi.org/10.1016/j.fuel.2009.10.007.
[29] Thiruvengadam A, Besch M, Padmanaban V, Pradhan S, Demirgok B. Natural gas vehicles in heavy-duty transportation-A review. Energy Policy 2018;122:253–9. https://doi.org/10.1016/j.enpol.2018.07.052.
[30] Karavalakis G, Hajbabaei M, Jiang Y, Yang J, Johnson KC, Cocker DR, et al. Regulated, greenhouse gas, and particulate emissions from lean-burn and stoichiometric natural gas heavy-duty vehicles on different fuel compositions. Fuel 2016;175:146–56. https://doi.org/10.1016/j.fuel.2016.02.034.
[31] Thiruvengadam A, Besch MC, Yoon S, Collins J, Kappanna H, Kappanna DK, et al. Characterization of particulate matter emissions from a current technology natural gas engine. Environ Sci Technol 2014;48:8235–42. https://doi.org/10.1021/es5005973.
[32] Napolitano P, Alfè M, Guido C, Gargiulo V, Fraioli V, Beatrice C. Particle emissions from HD SI gas engine fueled with LPG and CNG. Fuel 2020;269:117439. https://doi.org/10.1016/j.fuel.2020.117439.
[33] Singh AP, Pal A, Agarwal AK. Comparative particulate characteristics of hydrogen, CNG, HCNG, gasoline and diesel fueled engines. Fuel 2016;185:491–9. https://doi.org/10.1016/j.fuel.2016.08.018.
[34] Baratta M, Misul D, Xu J, Fuerhapter A, et al. Development of a high performance natural gas engine with direct gas injection and variable valve actuation. SAE Int J Engines 2017;10(5):2535–51. https://doi.org/10.4271/2017-24-0152.
[35] Standard ISO 4259: Petroleum and related products – Precision of measurement methods and results. 2017. 92 p.
[36] Zhiqin J. Dual-Fuel Combustion in aHeavy-Duty Engine. Thesis for the Degree of Doctor of Philosophy in Thermo and Fluid Dynamics. Chalmers University of Technology. 2018. 98 p. ISBN 978-91-7597-696-9.
[37] Swedish Standard SS-EN16723-2:2017. Natural gas and biomethane for use in transport and biomethane for injection in the natural gas network – Part 2: Automotive fuels specification. 2017. 36 p.
[38] Khatri, J. and Koopmans, L., "Water Injection System Application in a Mild Hybrid Powertrain," SAE Technical Paper 2020-01-0798, 2020, doi: 10.4271/2020-01-0798.
[39] Baratta, M., Rapetto, N., Spessa, E., Fuerhapter, A. et al., "Numerical and Experimental Analysis of Mixture Formation and Performance in a Direct Injection CNG Engine," SAE Technical Paper 2012-01-0401, 2012, doi: 10.4271/2012-01-0401.
[40] Heywood, J.B., "Internal Combustion Engine Fundamentals," McGraw-Hill: p. 960, 1988, ISBN-10: 007028637X.
[41] Standard ISO/IEC Guide 98-3:2008. Uncertainty of Measurement – Part 3: Guide to the expression of uncertainty in measurement (GUM:1995). 2008. 120 p.
[42] Song J, Choi M, Park S. Comparisons of the volumetric efficiency and combustion characteristics between CNG-DI and CNG-PFI engines. Appl Therm Eng 2017;121:595–603. https://doi.org/10.1016/j.applthermaleng.2017.04.110.
[43] Clasen, K. and Koopmans, L., "Investigation of Homogeneous Lean SI Combustion in High Load Operating Conditions," SAE Int. J. Adv. & Curr. Prac. in Mobility 2(4):2051-2066, 2020, doi: 10.4271/2020-01-0959.
[44] Tadesse, G. and Aziz, A., "Effect of Boost Pressure on Engine Performance and Exhaust Emissions in Direct-Injection Compressed Natural Gas (CNG-DI) Spark Ignition Engine," SAE Technical Paper 2009-32-0135, 2009.
[45] Baratta M., Ambrosio S., Misul D., Spessa E. Effects of H2 Addition to Compressed Natural Gas Blends on Cycle-to-Cycle and Cylinder-to-Cylinder Combustion Variation in a Spark-Ignition Engine. Journal of Engineering for Gas Turbines and Power. Vol. 136 (5). 2014 May: 12 p. Doi: 10.1115/1.4026163.
[46] Sevik J, Pamminger M, Wallner T, Scarcelli R, et al. Performance, efficiency and emissions assessment of natural gas direct injection compared to gasoline and natural gas port-fuel injection in an automotive engine. SAE Int J Engines 2016;9(2):1130–42. https://doi.org/10.4271/2016-01-0806.
[47] Lee J, Park C, Bae J, Kim Y, Lee S, Kim C. Comparison between gasoline direct injection and compressed natural gas port fuel injection under maximum load condition. Energy 2020;197:9. https://doi.org/10.1016/j.energy.2020.117173. 117173.
[48] Cho HM, He BQ. Spark ignition natural gas engines – A review. Energy Convers Manage 2007;48:608–18. https://doi.org/10.1016/j.enconman.2006.05.023.
[49] Lee S, Yi UH, Jang H, Park C, Kim C. Evaluation of emission characteristics of a stoichiometric natural gas engine fueled with compressed natural gas and biomethane. Energy 2021;220:11. https://doi.org/10.1016/j.energy.2021.119766. 119766.
[50] Ahmad Z, Kaario O, Karimkashi S, Qiang C, Vuorinen V, Larmi M. Effects of ethane addition on diesel-methane dual fuel combustion in a heavy-duty engine. Fuel 289 2021:12. https://doi.org/10.1016/j.fuel.2020.119834. 119834.
[51] Lee S, Kim C, Choi Y, Lim G, Park C. Emissions and fuel consumption characteristics of an HCNG-fueled heavy-duty engine at idle. Int J Hydrogen Energy 2014;39:8078–86. https://doi.org/10.1016/j.ijhydene.2014.03.079.
[52] Zhang M, Hong W, Xie F, et al. Experimental investigation of impacts of injection timing and pressure on combustion and particulate matter emission in a spray-guided GDI engine. Int J Automot Technol 2018;19:393–404. https://doi.org/10.1007/s12239-018-0038-8.
[53] Jiao Q, Reitz R. The Effect of Operating Parameters on Soot Emissions in GDI Engines. SAE Int J Engines 2015;8(3):1322–33. https://doi.org/10.4271/2015-01-1071.
[54] Kim T, Song J, Park J, Park S. Numerical and experimental study on effects of fuel injection timings on combustion and emission characteristics of a direct-injection spark-ignition gasoline engine with a 50 MPA fuel injection system. Appl Therm Eng 2018;144:890–900. https://doi.org/10.1016/j.applthermaleng.2018.09.007.
[55] Chintala V, Subramanian KA. A CFD (computational fluid dynamics) study for optimization of gas injector orientation for performance improvement of a dual-fuel diesel engine. Energy 2013;57:709–21. https://doi.org/10.1016/j.energy.2013.06.009.
[56] Herrera J., Toohey J., Jin B., Rogers T., Koopmans L. Effects of Different Port Injection CNG System Configurations on a 3.8L V6 Engine. ICSAT 2012. Proceedings of the 4th International Conference "Suistainable Automotive Technologies 2012": 103 – 109, doi 10.1007/978-3-642-24145-1.
[57] Raza M, Chen L, Leach F, Ding S. A review of particulate number (PN) emissions from gasoline direct injection (GDI) engines and their control techniques. Energies 2018;11:1417. https://doi.org/10.3390/en11061417.
[58] Hu N, Tan J, Wang X, Zhang X, Yu P. Volatile organic compound emissions from an engine fueled with an ethanol-biodiesel-diesel blend. J Energy Inst 2017;90:101–9. https://doi.org/10.1016/j.joei.2015.10.003.
[59] Etikyala, S., Koopmans, L., and Dahlander, P., "Particulate Emissions in a GDI with an Upstream Fuel Source," SAE Technical Paper 2019-01-1180, 2019, doi: 10.4271/2019-01-1180.
[60] Hora TS, Shukla PC, Agarwal AK. Particulate emissions from hydrogen enriched compressed natural gas engine. Fuel 2016;166:574–80. https://doi.org/10.1016/j.fuel.2015.11.035.
[61] Amirante R, Distaso E, Di Iorio S, Sementa P, Tamburrano P, Vaglieco BM, et al. Effects of natural gas composition on performance and regulated, greenhouse gas and particulate emissions in spark-ignition engines. Energy Convers Manage 2017;143:338–47. https://doi.org/10.1016/j.enconman.2017.04.016.
[62] Pirjola L, Dittrich A, Niemi JV, Saarikoski S, Timonen H, Kuuluvainen H, et al. Physical and chemical characterization of real-world particle number and mass emissions from city buses in finland. Environ Sci Technol 2016;50:294–304. https://doi.org/10.1021/acs.est.5b04105.
[63] Roesler JF, Martinot S, McEnally CS, Pfefferle LD, Delfau J-L, Vovelle C. Investigating the role of methane on the growth of aromatic hydrocarbons and soot in fundamental combustion processes. Combust Flame 2003;134:249–60. https://doi.org/10.1016/S0010-2180(03)00093-2.
[64] Kado NY, Okamoto RA, Kuzmicky PA, Kobayashi R, Ayala A, Gebel ME, et al. Emissions of toxic pollutants from compressed natural gas and low sulfur diesel fueled heavy duty transit buses tested over multiple driving cycles. Environ Sci Technol 2005;39:7638–49. https://doi.org/10.1021/es0491127.
[65] Überall A, Otte R, Eilts P, Krahl J. A literature research about particle emissions from engines with direct gasoline injection and the potential to reduce these emissions. Fuel 2015;147:203–7. https://doi.org/10.1016/j.fuel.2015.01.012.